Snake River Plain – Yellowstone silicic volcanism: implications for magma genesis and magma fluxes

WILLIAM P. LEEMAN[1], CATHERINE ANNEN[2] & JOSEF DUFEK[3]

[1]*National Science Foundation, Earth Sciences Division, 4201 Wilson Blvd, Arlington, VA 22330, USA (e-mail: wleeman@nsf.gov)*

[2]*Département de Minéralogie, University of Geneva, 1205 Geneva, Switzerland*

[3]*Department of Earth and Planetary Science, University of California, Berkeley, CA 94720, USA*

Abstract: The origin of large-volume, high-temperature silicic volcanism associated with onset of the Snake River Plain – Yellowstone (SRPY) hotspot track is addressed based on evolution of the well-characterized Miocene Bruneau–Jarbidge (BJ) eruptive centre. Although O–Sr–Pb isotopic and bulk compositions of BJ rhyolites exhibit strong crustal affinity, including strong ^{18}O-depletion, Nd isotopic data preclude wholesale melting of ancient basement rocks and implicate involvement of a juvenile component – possibly derived from contemporaneous basaltic magmas. Several lines of evidence, including limits on ^{18}O-depletion of the rhyolite source rocks due to influx of meteoric/hydrothermal fluids, constrain rhyolite generation to depths shallower than mid-upper crust (<20 km depth). For crustal melting driven by basaltic intrusions, sustenance of temperatures exceeding 900 °C at such depths over the life of the BJ eruptive centre requires incremental intrusion of approximately 16 km of basalt into the crust. This minimum basaltic flux (*c*. 4 mm year^{-1}) is about one-tenth that at Kilauea. Nevertheless, emplacement of such volumes of magma in the crust creates a serious room problem, requiring that the crust must undergo significant extensional deformation – seemingly exceeding present estimates of extensional strain for the SRPY province.

This paper addresses two related issues – each of which carries important broader implications. The first concerns the origin of large-volume, high-temperature silicic magmas associated with the Yellowstone hotspot track. Assuming they form largely in response to intrusion of voluminous basaltic magma into the crust, we are interested in knowing how much basalt is required, and at what depths that magma is emplaced. Our approach is to evaluate the conditions required to elevate crustal temperatures to magmatic values over volumes that are sufficiently large to generate the quantities of magma produced. Also, many rhyolites from this province exhibit ^{18}O-depletion, and this characteristic is widely attributed to involvement of low-δ^{18}O meteoric waters. Assuming that this anomaly is source-related, the depths to which surface fluids can plausibly circulate and effectively alter the oxygen isotopic composition of large volumes of crust provide an important constraint on maximum depth of crustal melting. Thus, a second issue concerns how and where the magmas acquire this signal, and what significance this holds regarding both rhyolite petrogenesis and fluid flow in the crust. Although we focus mainly on the physical processes involved, an important side issue concerns the relative contributions of pre-existing crustal rocks v. basalt-derived components in forming the rhyolite magmas; this, in turn, bears on how much older crust is melted.

As a framework for the problem, discussion is centred mainly on the relatively well-characterized Miocene Bruneau–Jarbidge (BJ) volcanic field in the central Snake River Plain (cf. Bonnichsen *et al.* 2008). This area is examined because, unlike Yellowstone itself, (1) the entire cycle of BJ silicic magmatism has run to completion, and (2) all BJ rhyolites exhibit strong ^{18}O-depletion – collectively comprising the most voluminous occurrence of such magmas known in the world (Boroughs *et al.* 2005; Cathey *et al.* 2007). We envisage that the processes underlying BJ magmatism were repeated in a diachronous fashion as magmatism migrated laterally over time.

Two investigative approaches are combined to constrain the depth of rhyolite genesis. On one hand, the capacity of meteoric/hydrothermal fluids to modify a substantial volume of crust diminishes exponentially with depth (and decreasing crustal permeability) such that ^{18}O-depleted sources for BJ rhyolites are probably confined to the upper crust. On the other hand, even under optimal conditions, production of just the *minimal* estimated volume of BJ rhyolite requires rather extreme inputs of basaltic

From: ANNEN, C. & ZELLMER, G. F. (eds) *Dynamics of Crustal Magma Transfer, Storage and Differentiation*. Geological Society, London, Special Publications, **304**, 235–259.
DOI: 10.1144/SP304.12 0305-8719/08/$15.00

magma into the crust in order to maintain sufficiently high temperatures at those depths. The consequences of our models regarding crustal/lithospheric modification are profound and require confirmation by additional approaches.

Background: fundamental characteristics of the SRPY magmatic province

Volcano-tectonic overview

The Neogene Snake River Plain – Yellowstone (SRPY) province is one of the most prolific volcanic systems in the western United States. Volcanism can be generalized in terms of migration of a series of volcanic centres across southern Idaho (Fig. 1) starting in north-central Nevada (at *c*. 16.5 Ma) and progressing to the currently active Yellowstone Plateau (at *c*. 2 Ma) in northwestern Wyoming (Armstrong *et al.* 1975; Pierce & Morgan 1992). All eruptive centres in this province exhibit a two-stage history: first (1) an initial phase (lasting *c*. 2 to as much as 4 Ma) that produced voluminous high-silica rhyolite lavas and ignimbrites; then (2) a culminating phase of predominantly basaltic activity. Although onset of basaltic *volcanism* was delayed relative to appearance of the earliest rhyolites at any given centre, basaltic *magmatism* is inferred to be coeval with (or to have even preceded) the earliest rhyolites (cf. Hildreth *et al.* 1991). Bonnichsen *et al.* (2008) also inferred from widespread (over some 400 km) lateral distribution of Miocene (11–10 Ma) rhyolites that basaltic intrusions must have been similarly distributed in the crust by that time. Moreover, once initiated, basaltic eruptions continued intermittently – up to Quaternary time across much of the province. For example, the Yellowstone Plateau volcanic field is considered to be in

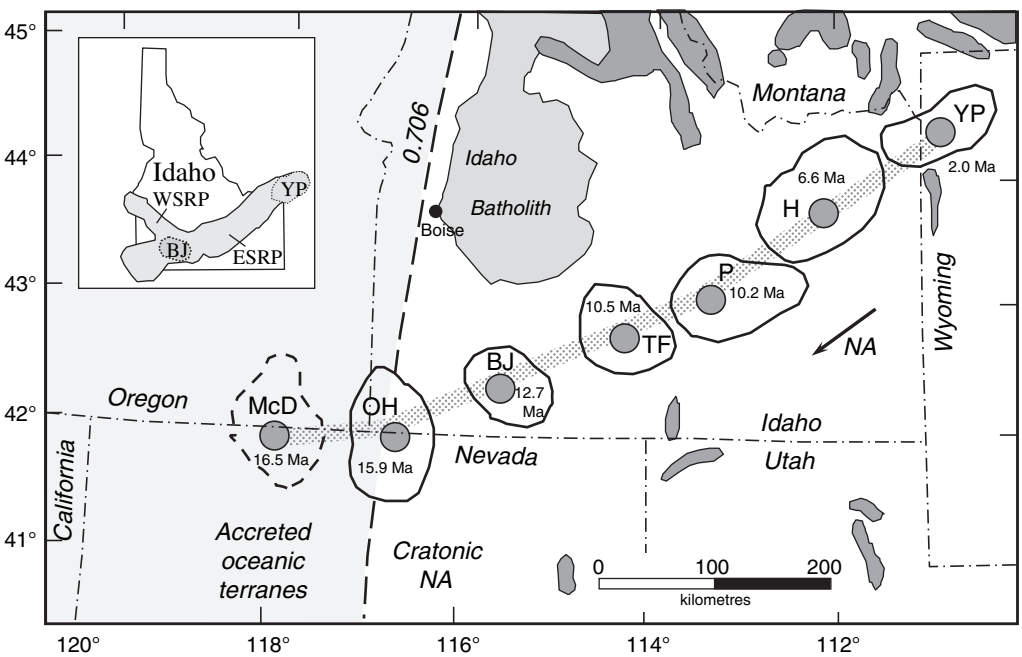

Fig. 1. Map showing general loci and ages of initial eruptions for silicic eruptive centres ascribed to activity of the Yellowstone 'hotspot' (after Pierce & Morgan 1991). These include (from oldest to youngest): McDermitt (McD), Owyhee-Humboldt (OH), Bruneau–Jarbidge (BJ), Twin Falls (TF), Picabo (P), Heise (H) and Yellowstone Plateau (YP). The Shaded line connects centroids of the eruptive centres; changes in azimuth relative to absolute motion of North America (arrow labelled NA; Gripp & Gordon, 2002) are probably artefacts of Neogene extensional deformation. Most of the Snake River Plain–Yellowstone province is underlain by Precambrian cratonic continental lithosphere that extends as far west as the $^{87}Sr/^{86}Sr = 0.706$ isopleth (Leeman *et al.* 1992); the region west of this line is underlain by accreted oceanic terranes of Phanerozoic age. The southern lobe of the Idaho batholith and surface exposures of Precambrian basement are shown in shaded fields. Inset shows loci of the BJ and YP centres superimposed on the physiographic area of the Snake River Plain province (WSRP and ESRP refer to western and eastern parts of the Snake River Plain). Nash *et al.* (2006) discuss possible implications of spacing of the volcanic centres.

the early part of its second phase, with most basaltic lavas confined to the last 0.5 Ma (Christiansen 2001). However, basaltic magmatism in this age range also occurred locally across the eastern and central SRP and as far west as the Boise area. Simply put, SRP basaltic magmatism did not follow a simple age – space progression.

Despite this, it is widely considered that the SRPY province could be a 'hotspot track' produced by migration of North America over an ascending mantle plume or melting anomaly that presently underlies the Yellowstone area (cf. Pierce & Morgan 1991). In support of this view, recent seismic tomographic studies document the presence beneath Yellowstone of a NW-dipping plume-like velocity anomaly that extends some 500 km into the upper mantle (Yuan & Duecker 2005; Waite *et al.* 2006). Nash *et al.* (2006) attempt to relate spacing of the volcanic centres to the presence of a plume-tail like feature with a diameter on the order of 70–100 km. However, the style of SRPY volcanism differs dramatically from that associated with oceanic 'hotspots', where magmatism generally follows simple age – distance progressions and is fundamentally basaltic in character. Magma generation processes in this setting probably are complicated by the presence of a thick continental lithospheric lid and cratonic crust that are inferred to extend as far west as the $^{87}Sr/^{86}Sr = 0.706$ isopleth as measured in Mesozoic to Neogene igneous rocks (cf. Leeman *et al.* 1992). These authors note that silicic volcanic rocks from centres (e.g. McDermitt) associated with the Snake River Plain trend, but that are situated west of the '0.706 line', have lower $^{87}Sr/^{86}Sr$; such compositional variations presumably reflect lateral heterogeneities in the crustal source rocks. As a step toward developing a comprehensive physical model for the SRPY magmatic province, here we evaluate the crustal-level processes responsible for the voluminous silicic magmatism and thereby indirectly estimate the required flux of basaltic magma driving the system.

Volume and scale of the rhyolite systems

A principle constraint is the volume of silicic magma that was produced over time. Each of the SRPY eruptive centres produced several large rhyolite ignimbrite eruptions of 'super volcano' class ($\geq$1000 km^3) along with multiple smaller ignimbrites and numerous lavas (Perkins *et al.* 1995; Morgan & McIntosh 2005). Currently, volumes are best known in the vicinity of Yellowstone and in the central Snake River Plain (Fig. 2).

Yellowstone Plateau (YP) At Yellowstone, it is clear that most rhyolitic eruptions were confined to a well-mapped set of nested calderas, the largest of which is approximately 75 km across in its longest dimension (Christiansen 2001). A variety of geophysical observations indicate the presence of a large magma body at depths between 6 and 10 km below the surface (Eaton *et al.* 1975; Smith & Braile 1994). Peripheral eruptions of rhyolite lavas and of minor Pleistocene and younger basalts suggest that the areal footprint of the overall magma system is roughly circular with a diameter on the order of 100 km. The cumulative volume of rhyolite extruded in the past 2 Ma at Yellowstone is estimated to be at least 6000 km^3 (Hildreth *et al.* 1991), not including widely dispersed airfall tephra or intracaldera fill. More than half of the total volume is represented by the large Huckleberry Ridge (at least 2500 km^3) and Lava Creek (*c.* 1000 km^3) tuffs, erupted at 2.03 and 0.64 Ma, respectively.

Central Snake River Plain (CSRP) Source regions for CSRP (acronym used to denote geographic area) silicic magmas are poorly exposed owing to subsidence and burial beneath younger sediments and extensive basalt flows. However, most ignimbrites in this area can be traced back to the so-called Bruneau Jarbidge (BJ; acronym used in referring to these specific volcanic rocks) volcanic centre (Fig. 1) – an area comparable in size and geometry to the Yellowstone Plateau volcanic field. In the eastern part of the map area, a number of younger ($<$10.2 Ma) ignimbrites overlap the BJ sequence; these presumably erupted from vents within the so-called Twin Falls volcanic field. Bonnichsen *et al.* (2008) suggest that, between 12.7 and 10.5 Ma, the BJ eruptive centre produced nine significant ignimbrites collectively comprising at least 7000 km^3 (based on estimated thickness of outflow deposits integrated over their known distribution area). By analogy with Yellowstone, this early stage is considered to be related to caldera-style eruptions. BJ ignimbrite episodes were generally more frequent than at Yellowstone, but separated by irregular lulls of 200–400 ka duration. Between 10.5 and 8.0 Ma, a change in eruptive style was attended by production of predominantly rhyolitic lavas with individual volumes ranging between 10 and 200 km^3. The first basaltic lavas (*c.* 9.5 Ma) of the BJ field further mark a distinctive developmental change in this eruptive centre. According to current interpretations (Pierce & Morgan 1991), the waning stage of the BJ centre was partly coeval with ignimbrite eruptions from the Twin Falls centre. However, it seems likely that there was a time-transgressive shift in the focus of magmatism.

Based on regional tephrochronology studies, Perkins & Nash (2002) estimate that the total volume of rhyolite produced from the CSRP

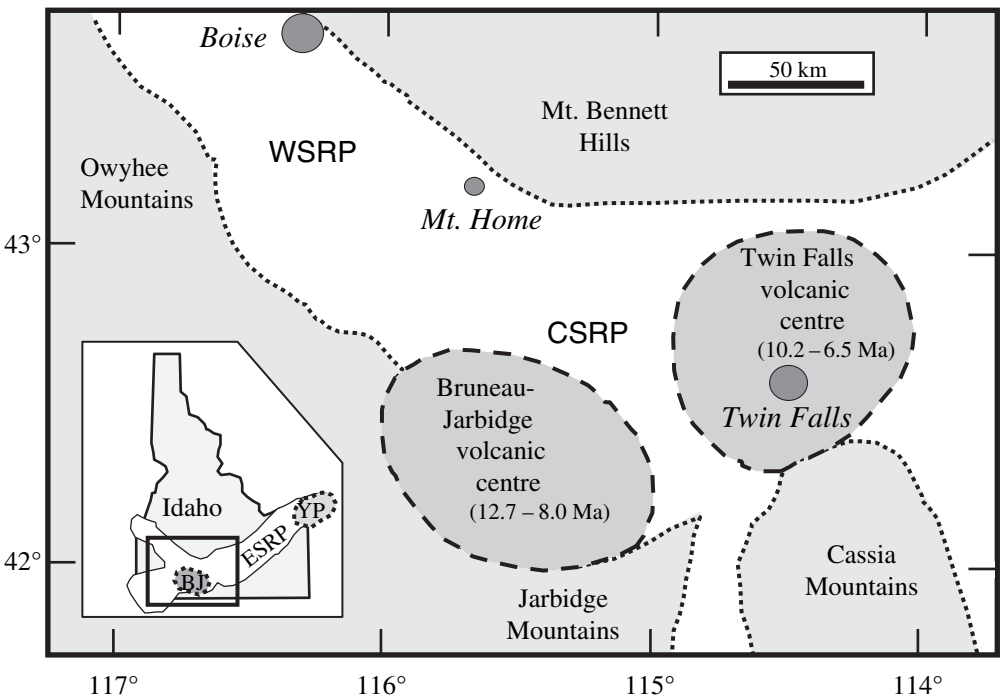

Fig. 2. Detailed map showing the main focal area of this paper in the western and central Snake River Plain. Location of this area with respect to the broader Snake River Plain (SRP) is indicated in the inset (labels as in Fig. 1). We emphasize relations in the Bruneau–Jarbidge (BJ) volcanic centre that is representative of the greater central Snake River Plain (CSRP) region. We also discuss data from the northeastern flank of the Owyhee Mountains. Shaded circles indicate principal towns. The topographically low SRP is surrounded by highlands shown as shaded pattern.

(between 12.7 and 8.0 Ma) could have exceeded 10 000 km^3. The total volume of silicic magma produced should also include an unknown quantity of equivalent intrusive material; by analogy with other treatments (cf. Crisp 1984) this could amount to several times the extrusive volume. Here, we consider alternative volume production scenarios in which the intrusive:extrusive magma ratio is set conservatively at 2:1. Using estimates of extruded volume (7000–10 000 km^3), this approach implies a total magma volume on the order of 21 000–30 000 km^3. For comparison, the equivalent volume for the Yellowstone Plateau volcanic field could exceed 10 000 km^3 (Hildreth *et al.* 1991).

Minimal magma production estimates for the CSRP are summarized in Table 1 and illustrated in Figure 3. Magma production clearly was non-linear over time. The early ignimbrites and related deposits comprise about 75% (>5000–7500 km^3) of the total effusive products, whereas the younger lavas comprise the remainder. The ignimbrite episodes also appear to have varied greatly in volume output, with more than half associated with the three largest units (Cougar Point tuffs VII, XI and XIII, all with volumes exceeding 1000 km^3).

Rhyolite petrology and temperature

CSRP rhyolites are almost exclusively metaluminous in composition, with SiO_2 contents between 71 and 76% for most. With few exceptions, they carry distinctively anhydrous phenocryst assemblages, including plagioclase ± sanidine ± quartz + magnetite ± ilmenite + pigeonite + augite ± orthopyroxene ± fayalite with accessory zircon and apatite. Amphibole and biotite are conspicuously lacking. A variety of mineral thermometers (two-pyroxene, two-feldspar, two-oxide and Ti in quartz) demonstrate that magmatic temperatures typically exceeded 900 °C and in some cases reached 1000 °C (Honjo *et al.* 1992; Cathey & Nash 2004; Leeman, unpublished data). Yellowstone rhyolites are generally similar. Although mineral temperatures tend to be somewhat lower (800–900 °C) for most units, a few approach 1000 °C (Hildreth *et al.* 1984; Leeman, unpublished data). Rare amphibole (e.g. in member A of the Lava Creek tuff) is consistent with slightly higher volatile content and/or lower temperature for very few units, but otherwise SRPY rhyolite magmas are significantly hotter than those from other

Table 1. *Volume of rhyolite erupted from the CSRP (Bruneau–Jarbidge volcanic centre)*

CAT Group	Main BJ units	Main product	Age range (Ma)	Volume (km^3)	Total volume (%)	Cumulative volume (%)	Effusion rate (km^3/Ma)
1	CP III	ign	12.8–12.4	100	1.4	1.4	250
2	CP V	ign	12.4–11.9	300	4.3	5.7	600
3	CP VII	ign	11.9–11.7	1200	17.1	22.9	6000
4	CP IX	ign	11.7–11.5	300	4.3	27.1	1500
5	CP XI	ign	11.5–11.2	1800	25.7	52.9	6000
6	CP XII	ign	11.2–11.0	200	2.9	55.7	1000
7	CP XIII	ign	11.0–10.7	1800	25.7	81.4	6000
8	CP XV	ign	10.7–10.4	200	2.9	84.3	667
9	CT	ign	10.4–10.0	100	1.4	85.7	250
10	LD-BJ	lf	10.0–9.5	200	2.9	88.6	400
11	SC	lf	9.5–9.0	400	5.7	94.3	800
12	DC	lf	9.0–7.5	300	4.3	98.6	200
13	SF	lf	7.5–5.5	100	1.4	100.0	60

Note: volumes are based on stratigraphic data of Bonnichsen *et al.* (2008) and exclude distal tephras and intracaldera fill; volume is given as a percentage of total, which is estimated to be between 7000 and 10 000 km^3.
CAT groups include chemically similar units erupted within the indicated time intervals.
Principal eruptive units include Cougar Point Tuffs (CP) and large rhyolite lavas: Cedar Tree (CT), Long Draw (LD), Bruneau Jasper (BJ), Sheep Creek (SC), Dorsey Creek (DC) and Shoshone Falls (SF); basaltic lavas first appear between CAT Groups 10 and 11. Products: ignimbrite (ign), lava flow (lf).

settings in the Cordilleran United States. (Christiansen & McCurry 2008).

Rhyolite compositional variation with time

Here we emphasize compositional variations in rhyolitic products of the CSRP based on detailed studies of selected stratigraphic sections, extensive chemical analyses, and new $^{39}Ar/^{40}Ar$ dating of critical units as synthesized by Bonnichsen *et al.* (2008). Data from three distal areas were compared on the basis of averaged analyses for individual units, and stratigraphic correlations based on all available data. The temporal evolution of the magmatic system is exemplified by data from the BJ volcanic centre proper.

Figure 4 portrays temporal variation in selected compositional parameters. All element concentration or ratio data represent unit averages; isotopic data are individual sample analyses. Notably FeO^T, TiO_2 and $^{143}Nd/^{144}Nd$ (also $^{87}Sr/^{86}Sr$, Sr, Nb, Y – not shown) display fairly systematic increases with time whereas highly incompatible elements and related ratios (e.g. Rb, Rb–Sr) decrease. The observed trends are antithetical to those expected as a result of fractional crystallization control, albeit minor reversals (e.g. near 11.8, 11.1, 9.5 and around 8 Ma) could signify magmatic differentiation during interludes in eruptive activity. In essence, the rhyolites evolved to less differentiated compositions with time.

The overall pattern could be attributed to progressive melting of a common crustal reservoir except that Nd isotopic data require some degree of open system behaviour that causes rhyolite $^{143}Nd/^{144}Nd$ values to shift toward the observed basalt range over time. This shift is unlikely to involve simple mixing of basaltic and rhyolitic magmas because initial $^{87}Sr/^{86}Sr$ ratios are around 0.709 in the earliest rhyolites and increase to > 0.712 in the youngest lavas, becoming progressively *more* radiogenic than the basalt range (*c.* 0.706–0.707; cf. Menzies *et al.* 1984) over time. Nevertheless, mixing between pure crustal melts and derivative liquids produced from basaltic magma emplaced in the crust is likely to influence compositions of the erupted rhyolites (Hildreth *et al.* 1991; Annen & Sparks 2002). This topic is revisited shortly.

As a final comment, the 'reverse fractionation' trend documented for the BJ magma system appears to be unique compared with other magmatic centres associated with the Yellowstone melting anomaly (Bonnichsen *et al.* 2008). In many respects it resembles the bottom-to-top compositional zoning commonly observed in individual ignimbrites (Hildreth 1981) but, because this trend developed over an order of magnitude longer time scale, it is unlikely to result from evolution within a single long-lived magma chamber (Vazquez & Reid 2002).

Rhyolite sources: evidence for a dominant crustal component

Although protoliths for SRPY rhyolite magmas are uncertain, diverse evidence leaves little doubt that

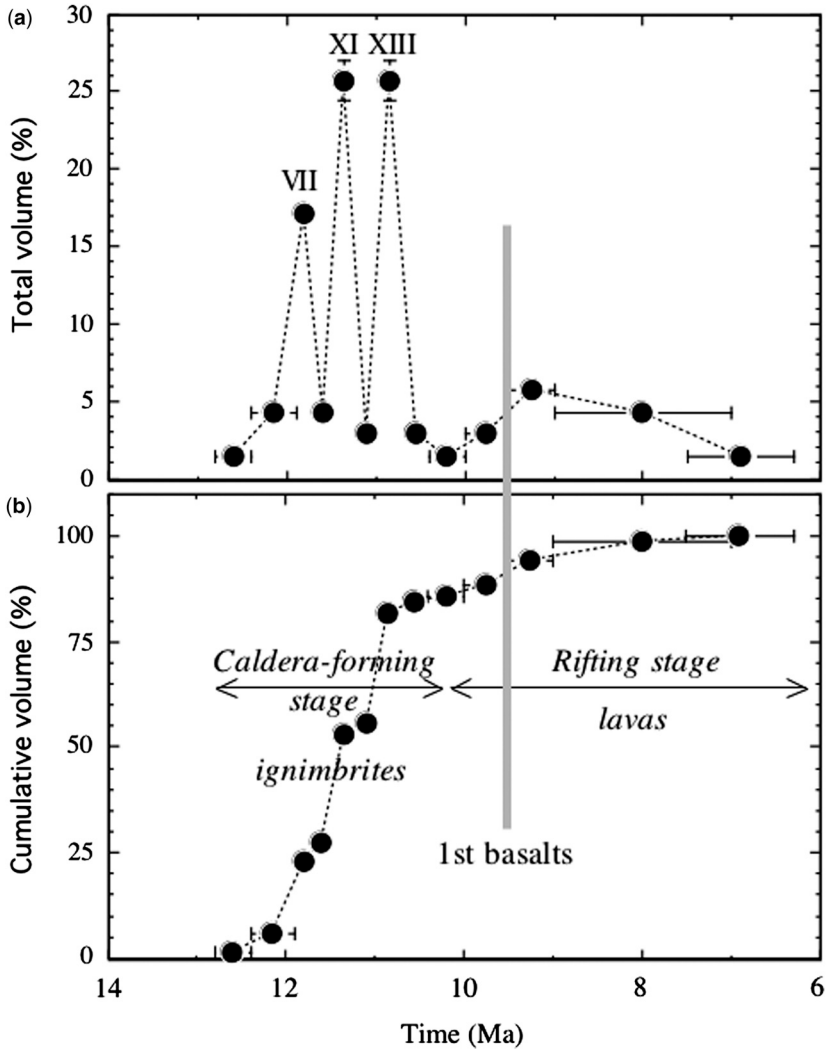

Fig. 3. Temporal variation in relative (**a**) and cumulative volume (**b**) of rhyolitic magma extruded from the Bruneau–Jarbidge eruptive centre; these are shown as percentages of the total volume excluding intracaldera fill and distal airfall deposits (for which volumes are unknown). Bonnichsen *et al.* (2008) estimate minimum volume to be at least 7000 km^3; Perkins & Nash (2002) suggest that total volume may have exceeded 10 000 km^3. Eruption rates and volumes were clearly highest between 12 and 10 Ma ('caldera-forming' stage), with notable spikes corresponding to three 'supervolcano scale' ignimbrite events, each having a volume in excess of 1000 km^3 (CPT units VII, XI and XIII). Appearance of the first basaltic eruptions (indicated by vertical line) closely coincides with a shift in eruption style to predominantly rhyolite lavas after 10 Ma ('rifting' stage).

these melts were largely derived by crustal melting. In most regards, SRPY rhyolites exhibit strong similarities to so-called A-type (or 'anorogenic') granitoids. Origins of such magmas have been discussed in detail by Patiño-Douce (1997), who noted that their high magmatic temperatures, metaluminous compositions and other geochemical characteristics are consistent with melting of relatively water-poor calcalkalic igneous rocks at low pressures (<5 kbar) within the shallow crust. He also presented analyses of partial melts of tonalite (30–40% melting) and granodiorite (*c.* 20% melting) bulk compositions produced at 950 °C and 4 kbar that closely resemble compositions of SRPY rhyolites. A critical factor appears to be low pressure because melts produced at 8 kbar

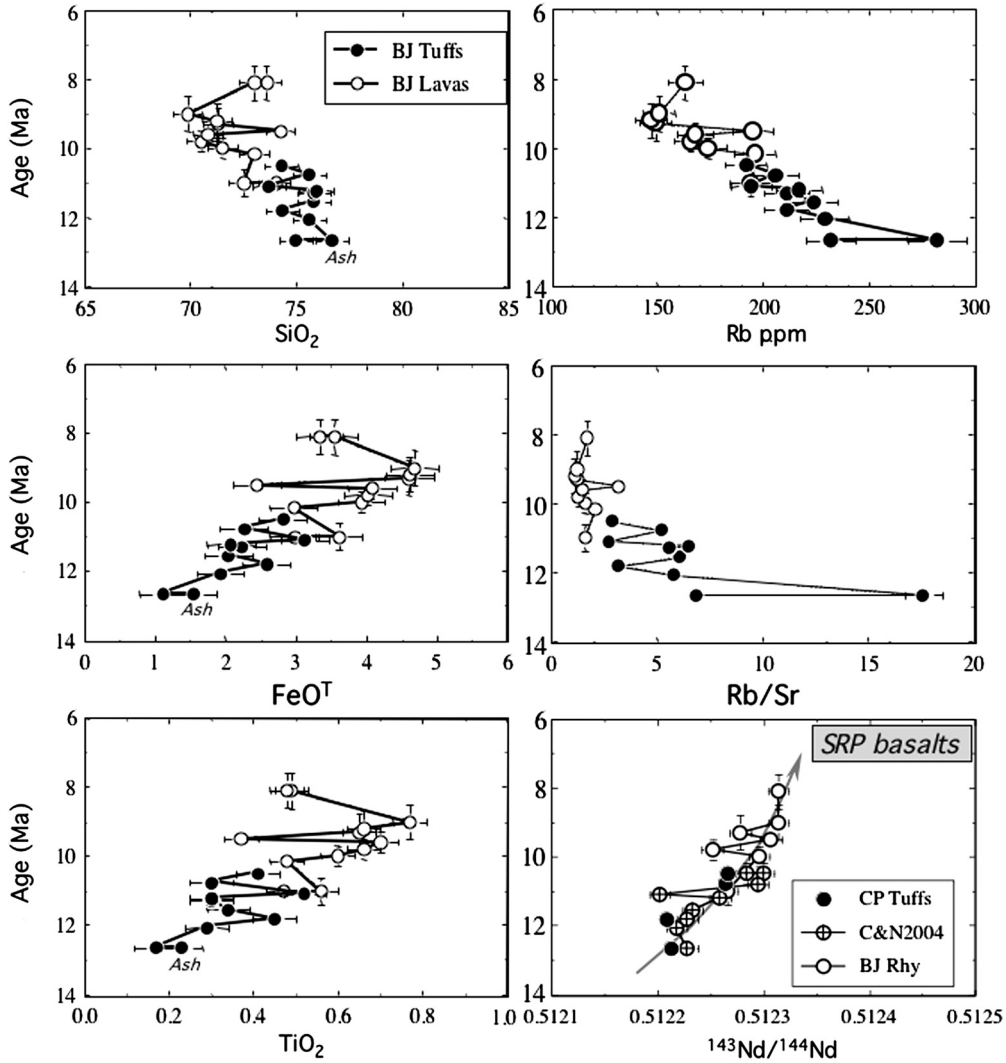

Fig. 4. Compositional variations in BJ rhyolite tuffs and lavas as a function of time. Unit averages are plotted from Bonnichsen *et al.* (2008), with additional Nd isotopic data for BJ tuffs from Cathey & Nash (2004); error bars reflect uncertainties in radiometric ages and standard deviations on unit averages. Nd isotopic data for SRP basalts are from Menzies *et al.* (1984) and Leeman (unpublished data).

have quite distinctive compositions owing to different residual mineral assemblages. Below, we evaluate model parameters required to consistently sustain the requisite high temperatures within shallow domains of the crust.

Differentiation of basaltic magmas also could generate some rhyolitic magma (McCurry *et al.* 2008), but it is unlikely that SRPY rhyolites could be produced *principally* by this process. In addition to geochemical inconsistencies noted below, there are problems with the large amounts of basalt required and the paucity of intermediate composition magmas as discussed by Bonnichsen *et al.* (2008).

Trace element constraints Bonnichsen *et al.* (2008) demonstrate that strongly to moderately incompatible elements in SRPY rhyolites exhibit similar enrichment levels when normalized to the average crustal composition of Taylor & McLennan (1985). Ignoring elements that are readily influenced by crystallization of observed phenocrysts or accessory phases (e.g. Sr, Ba, Eu), enrichment levels in BJ rhyolites are consistent with 15–25%

partial melting of sources similar to average crust. Data for Yellowstone and other SRP eruptive centres are similar (Hildreth *et al.* 1984, 1991; Hughes & McCurry 2002; Wright *et al.* 2002). For purposes of our modelling, we consider this range realistic for melt fraction (F) in the crust, and inferred source volumes may be calculated as estimated eruptive volume (see Table 1) divided by *F*. For simplicity, an average *F* value of 0.25 was adopted in estimating source volume. Larger *F* values imply smaller source volume estimates, and the effects of changing this parameter are illustrated later.

Radiogenic isotope constraints The Sr–Nd–Pb isotope geochemistry of SRPY rhyolites is distinctive in several respects (Doe *et al.* 1982; Hildreth *et al.* 1991; Leeman *et al.* 1992; Nash *et al.* 2006; Bonnichsen *et al.* 2008). Virtually all are characterized by elevated $^{87}Sr/^{86}Sr$ (>0.709) and low $^{143}Nd/^{144}Nd$ (<0.5123) compared with associated basalts. Pb isotopic ratios are varied, with $^{206}Pb/^{204}Pb$ ranging from unradiogenic (<17.5) near Yellowstone to progressively more radiogenic (*c*. 19.0) in the CSRP area. $^{206}Pb/^{204}Pb$–$^{207}Pb/^{204}Pb$ data define a near-linear array, the slope of which conforms to an Archaean (*c*. 2.5 Ga) secondary isochron (Leeman, unpublished data). Whether or not this array has strict age significance, the Pb data are consistent with incorporation of significant amounts of old craton-derived crustal Pb in the rhyolite source domain (e.g. Leeman *et al.* 1985; Wooden & Mueller 1988). On the other hand, Nd isotopic data for SRPY rhyolites are more radiogenic (typically, $\varepsilon_{Nd} > -10$) than compositions of Archaean basement rocks ($\varepsilon_{Nd} < -30$) in the region (Leeman *et al.* 1985). Much the same was observed at Yellowstone, although some extracaldera rhyolites have ε_{Nd} values as low as −18 (Hildreth *et al.* 1991). Overall, these data preclude wholesale melting of Archaean crust and seemingly require involvement of a more juvenile (i.e. recently mantle-derived) Nd component in most of the rhyolites (Nash *et al.* 2006).

Oxygen isotope constraints Oxygen isotopic compositions of SRPY rhyolites vary significantly and clearly point to open system modification of crustal source materials. Based on analyses of quartz, feldspar and zircon phenocrysts, most Yellowstone rhyolites have normal or only slightly depleted magmatic $\delta^{18}O$ (*c*. 5–8‰), and some are extremely depleted (with $\delta^{18}O < 2$‰). The latter typically followed major caldera collapse events (Hildreth *et al.* 1984); in these cases, the magmatic oxygen isotopic composition is thought to reflect assimilation (Hildreth *et al.* 1984; Balsley & Gregory 1998) or remelting (Bindeman & Valley 2001*a*) of low-$\delta^{18}O$ hydrothermally altered older volcanic rocks that subsided catastrophically into the underlying magma reservoir; Hildreth *et al.* (1984) also consider direct ingress of low-$\delta^{18}O$ hydrothermal brines into silicic magmas as a plausible alternative. However, recent oxygen isotopic analyses and U–Pb dating of zircons indicates that the assimilated/melted material is mainly cannibalized or recycled from early parts of the Yellowstone magmatic system rather than much older crustal rocks (Bindeman & Valley 2001*b*; Vazquez & Reid 2002). A similar picture has emerged for the slightly older Heise volcanic centre, except that there the earliest ignimbrites have fairly normal $\delta^{18}O$ values and low $\delta^{18}O$ rhyolites are restricted to the youngest, albeit voluminous, Kilgore ignimbrite as well as subsequent post-caldera rhyolite lavas (Bindeman *et al.* 2007).

In dramatic contrast, nearly all rhyolites, including the earliest ones, from the BJ and related eruptive centres in the CSRP, are characterized by $\delta^{18}O$-depletion (magmatic values near −1.4 to +3.8‰, based on feldspar and quartz analyses; Boroughs *et al.* 2005). Interestingly, partly contemporaneous rhyolites from the Owyhee Front (some 100 km to the NW) have normal $\delta^{18}O$ (7–9‰). The BJ results are confirmed by analyses of zircons from the Cougar Point tuffs (Cathey *et al.* 2007). These authors discount assimilation of low-$\delta^{18}O$ crustal materials by rhyolite magmas as the primary cause for ^{18}O-depletion; rather, their oxygen composition must be inherited from the respective magma sources. Boroughs *et al.* (2005) attribute CSRP rhyolite compositions to melting of Idaho batholith granitic rocks that were hydrothermally altered during the Eocene (Criss & Fleck 1987), and suggest that the Owyhee Front rhyolites are melts of similar lithologies that somehow escaped alteration. In any case, this work implies that much of the oxygen in these rhyolites is crustal in origin, and that very large volumes of the underlying crust have been modified by interaction with low-$\delta^{18}O$ waters, presumably of near-surface origin. Although subsequent events, like those at Yellowstone or Heise, could have contributed to the observed ^{18}O-depletion effects, extensive crustal modification must have preceded generation of the earliest rhyolite magmas. This critical observation dictates that extensive crustal melting occurred at shallow depths, within reach of infiltrating meteoric/hydrothermal waters.

Relative crustal and mantle (i.e. basaltic) contributions to BJ rhyolites

Of critical petrogenetic concern is the relative contribution of crust v. mantle components to SRPY rhyolite magmas. Specifically, what fraction of the

erupted magma derives from remelting of old pre-existing crust? To address this question we consider variations in O and Nd isotopic and selected major element data for BJ rhyolites in Figure 5. The composition of the 'purest' crustal-derived rhyolite ('C') is approximated by the most ^{18}O-depleted samples: $\delta^{18}O = c.\ 0‰$, Nd = 65 ppm, $\varepsilon_{Nd} = -8.4$. Major element composition for 'C' was based on partial melt of granodiorite at 4 kbar (Patiño-Douce 1997): $SiO_2 = 74.1\%$, $FeO^T = 2.2\%$. BJ area basalt compositions vary somewhat, but a representative analysis ('B') is as follows: $\delta^{18}O = 5.5‰$, Nd = 33 ppm, $\varepsilon_{Nd} = -3.7$, $SiO_2 = 47\%$, $FeO^T = 14\%$ (Leeman, unpublished data). Simple mixing models between these end member compositions (Fig. 5) provide a gauge for estimating crustal pedigree.

The rhyolite data define broad trends that deviate from simple end member mixing. As discussed earlier, part of the skewness in the $\delta^{18}O$ plots relates to inherent variations in oxygen composition of the rhyolite sources, but the Nd data most likely reflect open system mixing processes. Low FeO^T and high SiO_2 as well as lower ε_{Nd} in the BJ ignimbrites (tuffs) preclude a significant basalt contribution (perhaps $<10\%$) in the most voluminous rhyolites, whereas compositions of the relatively small volume rhyolite lavas are shifted toward expected differentiation products (or remelts) of the basaltic end member. Although inferred mixing proportions depend strongly on assumed end member composition(s), basalt-derived melt components plausibly could contribute as much as half the mass of the more iron-rich rhyolites (i.e. the late stage lavas). As seen in Figure 4, temporal increases in FeO^T and ε_{Nd} suggest that basaltic contributions increased as the BJ system matured. This observation is in accord with increased availability of basaltic magma (and its derivative liquids) for mixing with crust-derived melts over time. Considering the volumetric dominance of early ignimbrites (5900 km^3 or *c.* 85% erupted before 10.5 Ma; Table 1) over the younger rhyolite lavas (1100 km^3 or *c.* 15% after 10.5 Ma), it is possible to evaluate these contributions. Assuming roughly 10% (or *c.* 590 km^3/2.2 Ma = 268 km^3/Ma) basalt-derived melt contribution during the early stage and 50%

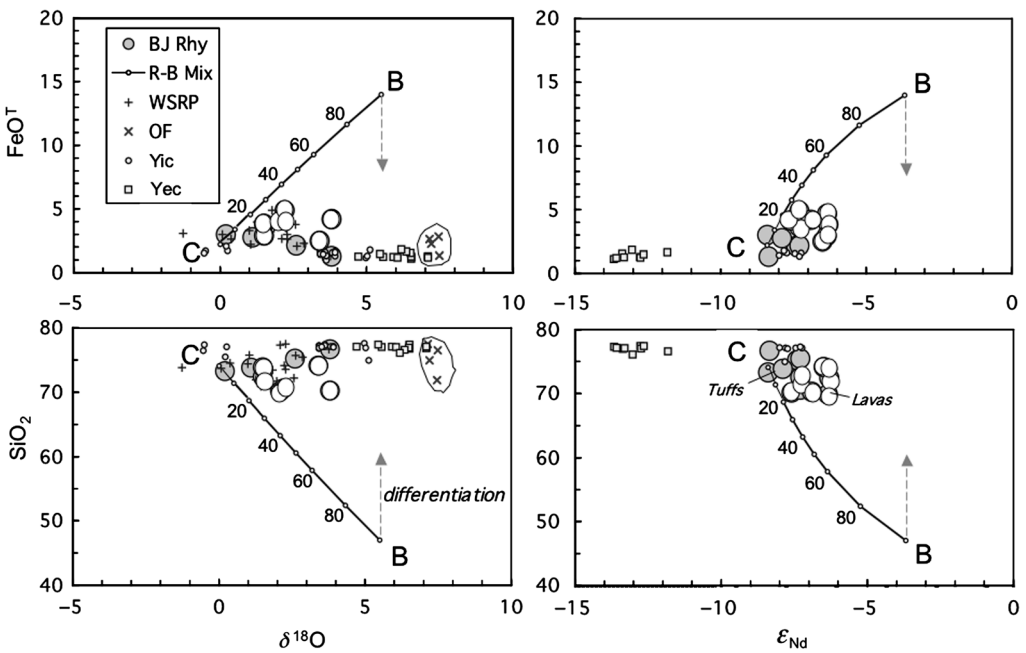

Fig. 5. Isotope systematics in rhyolites from the Bruneau–Jarbidge (BJ) area (Bonnichsen *et al.* 2007). Trajectories are shown for mixing between representative SRP basalt ('B') and crustal-derived liquids ('C') as represented by the most ^{18}O-depleted BJ rhyolite. Large circles represent BJ rhyolites: ignimbrites (shaded), lavas (white). Comparative data are shown for rhyolites from the WSRP (+) and Owyhee Front (×), and for intra- (small circles) and extra-caldera (small squares) rhyolites from Yellowstone (data from Hildreth *et al.* 1991; Boroughs *et al.* 2005). Dashed arrows schematically show expected trends for differentiation of primitive basaltic magmas and/or point toward compositions of silicic melts produced by remelting basaltic intrusive rocks.

(or *c*. 550 km^3/2.5 Ma = 220 km^3/Ma) during the late stage suggests that absolute contribution was nearly constant over time. Thus, temporal changes in BJ rhyolite chemistry could plausibly reflect variations in crustal melt production superimposed on a steady 'background' input of basalt-derived melts.

In comparison, data for Yellowstone and Owyhee Front rhyolites (Fig. 5) seemingly do not require large basaltic contributions. However, Hildreth *et al.* (1991) suggest that significantly higher ε_{Nd} values in intracaldera v. extracaldera rhyolites from Yellowstone probably reflect greater basaltic inputs proximal to the centre of the volcanic field.

Evidence for basalt intrusion in the middle–upper crust

Although basaltic volcanism is always posterior to the main episode of rhyolite volcanism, mafic magma needs to be involved in the generation of the rhyolites either as a parent or as a heat source to induce partial melting of the crust. Geophysical studies suggest the presence of a mafic body in the crust. A roughly 10 km thick, high-*Vp* lens has been seismically imaged in the middle crust between *c*. 9 and 19 km depth beneath the eastern SRP (Sparlin *et al.* 1982; Peng & Humphreys 1998); recent tomographic studies (Dueker *et al.* 2007) revise its depth downward to 15–25 km. This feature has been interpreted as a basaltic sill complex (Smith & Braile 1994; Shervais *et al.* 2006); there are insufficient seismic data to define its lateral extent.

Phase equilibria experiments on SRP basalts (Thompson 1975) and petrographic observations support the idea that these magmas commonly evolved at such shallow depths. Specifically, SRP basalts carry phenocryst assemblages of olivine $\pm$ plagioclase, consistent with crystallization at pressures less than *c*. 8 kbar (Leeman & Vitaliano 1976). Notably, the basalts conspicuously lack phenocrysts of clinopyroxene, whereas experimentally this mineral is found to be the primary liquidus phase in such magmas at pressures greater than 8–10 kbar, corresponding to the lower crust or uppermost mantle. Although geochemical evidence allows that many SRP basalts could have experienced 'cryptic' clinopyroxene crystallization at greater depths (Hildreth *et al.* 1991), the prevailing petrographic evidence indicates that most SRP basalts *last* segregated from storage reservoirs shallower than 25 $\pm$ 3 km. Although this does not preclude storage of some basalt in the deeper crust, no basalt originating directly from such depths has been identified so far.

Positive Bouguer gravity and magnetic intensity anomalies associated with the SRP (Mabey 1982; Smith & Braile 1994) support the concept that relatively shallow basaltic intrusion has significantly modified parts of the underlying crust. This idea is supported by long-wavelength isostatic residual gravity and magnetic potential maps (figs 8 & 18 of Mankinen *et al.* 2004) that effectively illuminate positive mass and magnetic anomalies at mid-crustal depths beneath much of the SRP and show that these anomalies are largely confined to the physiographic province (*c*. 100 km wide by 600 km long). Magmatic densification of the crust is also supported by available seismic refraction studies (Hill & Pakiser 1967; Pakiser 1991). Available data indicate a westward thickening of the higher-*Vp* lower crust (at the expense of the upper crustal layer), whereas overall crustal thickness remains nearly constant (*c*. 40 km beneath the entire province (Leeman 1982; Smith & Braile 1994). These relations are consistent with a greater relative proportion of high velocity and high density material in the crust beneath the western SRP, and we propose this to be an artefact of basaltic intrusion and extraction of voluminous rhyolite. Unfortunately, crustal structure in that region remains to be investigated in detail.

Physical models of magma generation

To generate rhyolite magmas, basalt must intrude, heat, and partially melt the crust. Furthermore, we assume that the source domain must have been altered by meteoric water. The infiltration of near-surface fluids is probably limited by decreasing crustal permeability with depth (Ingebritsen & Manning 1999). However, as we will see, it is difficult to sustain elevated temperatures (>900 °C) equivalent to the hottest rhyolites at shallow crustal depths. Thus, thermal and oxygen isotopic data together provide potentially powerful constraints on the possible depths of rhyolite magma generation. How these two factors might realistically be reconciled is addressed below.

A conceptual magma reservoir model

The observed transition from rhyolitic to basaltic volcanism in the SRPY province may be explained in terms of the role of the underlying continental crust as a low-density barrier that effectively traps ascending basaltic magmas during early stages of magmatism. Although Kavanagh *et al.* (2006) showed that density is not the only parameter that controls formation of sills into an elastic medium, buoyancy clearly is a driving force for the ascent of magmas and, on a crustal scale, must influence the final level where magmas stall and crystallize. A buoyancy model is considered here in which

representative densities are assumed for upper (2.6 kg dm^{-3}) and lower (2.9 kg dm^{-3}) crust, mantle (3.2 kg dm^{-3}), basaltic magma (2.7 kg dm^{-3}) and equivalent gabbro (2.9 kg dm^{-3}). In the simplest view, basaltic magma detached from a mantle source would be expected to ascend buoyantly into the crust and form sill-like lenses at depths where neutral buoyancy is favoured (cf. Ryan 1987), such as near the boundary between upper and lower crust. However, because cooling and solidification will produce denser gabbroic rock, subsequent batches of basaltic magma would tend to be emplaced above the growing sill complex (Fig. 6a). Not only will this process increase the overall density of the crust, but the proportion of crust having lower-crust density also will increase at the expense of the original upper crust domain. Although depths of magma stagnation (Z) in the crust could differ in detail from the above scenario for a variety of reasons, the proposed intrusive scenario provides a useful conceptual framework for thermal modelling presented below.

Based on the petrologic and experimental constraints summarized earlier, it is clear that most erupted SRPY basalts last evolved at depths shallower than 25 ± 3 km. Consideration of rhyolite generation (discussed below) and revised position of the seismically imaged sill complex both point to basaltic intrusion as shallow as 10–15 km depth. Given their density contrast relative to upper crustal rocks, basaltic magmas trapped at such mid-crustal depths would have little buoyancy incentive to rise much higher or to erupt, and would ultimately crystallize and heat the surrounding wall rocks.

As an interesting corollary, the onset of basaltic eruptions some 2 Ma after initial magmatism is consistent with time-progressive densification of normal continental crust. In its simplest form, the problem concerns how to sustain a magma column height (H) such that it exceeds the depth of the magma reservoir (Z) below the surface (Fig. 6b). H is computed simply as a function of magma density and lithostatic pressure at depth Z. It can be shown (Fig. 6c) that positive (H–Z) (i.e. eruption) is favoured by increasing reservoir depth or thinning

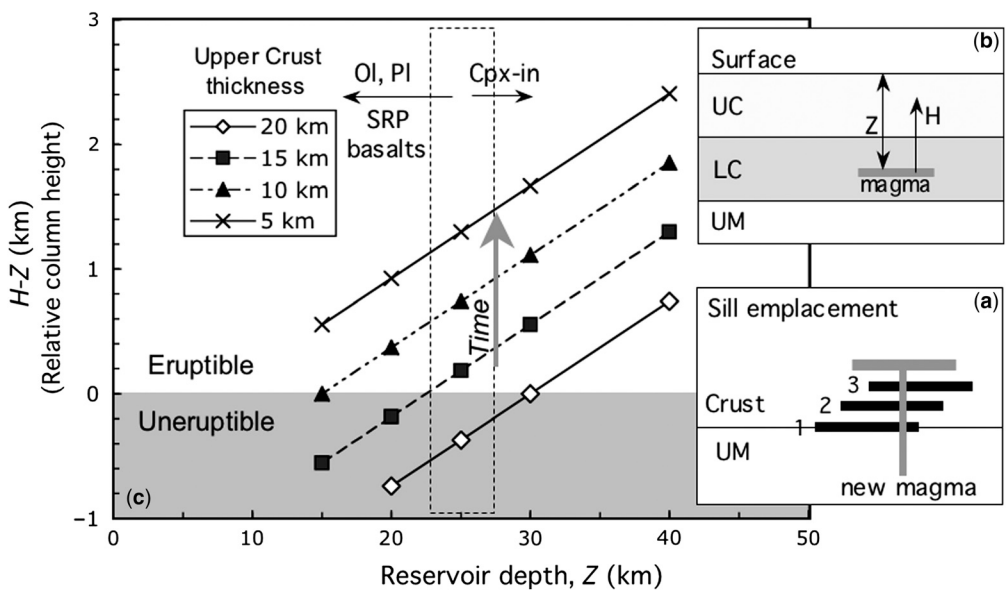

Fig. 6. Schematic diagram relating magma storage depths and ascent scenarios. (**a**) Overaccretion concept: basaltic magma ascends from the mantle and is emplaced as successive sills in the crust; density considerations favour emplacement of new magma above earlier, now denser intrusions emplaced in order of numbers. (**b**) Schematic/terminology: height (H) of a magma column originating from a reservoir at depth (Z) will vary depending on the density structure of the overlying crustal rocks; positive H–Z = eruption. (**c**) Model: H–Z relations for basaltic magma as functions of reservoir depth and thickness of overlying rocks with upper crustal density. With sustained mafic intrusion, the thickness of effective upper crust density layer will decrease with time, causing the relation between relative column height and reservoir depth to shift upward (indicated by vertical arrow). The dashed rectangle outlines maximum depth range for erupted SRPY basalts that is compatible with the pressure stability of observed olivine + plagioclase phenocryst assemblage. The absence of clinopyroxene phenocrysts limits Z values to shallower than 25 ± 3 km (see text for details).

of the effective upper crust density domain (hereafter, simply called 'upper crust'). However, if SRPY basalts are constrained to rise from reservoirs shallower than 25 km, they can only reach the surface if the effective density of the upper crust is increased sufficiently to overcompensate the mass of the magma column. This implies that some basalt is intruded within the shallow upper crust and/or mass is redistributed internally within the upper crust by some other means. An important process to increase upper crustal density could be extraction and upward migration of silicic magmas. Also, as discussed by Hildreth (1981), the mere presence of voluminous silicic magma bodies or partial melt zones in the upper crust (e.g. as inferred for Yellowstone today) would probably impede ascent of basaltic magma to the surface; solidification of such intercepted magmas would increase upper crustal density.

While over-pressurized magma chamber conditions at depth could modify these calculations, the general relations should be valid regardless of the chamber pressure conditions. For basaltic magmas to erupt from reservoirs as shallow as 15 km (top of the geophysically defined sill complex), the low-density upper crust domain must be less than *c*. 10 km thick to provide sufficient buoyancy lift. This intrusion model would consistently produce the observed phenocryst assemblage in SRPY basalts as long as new magma was emplaced near the top of the sill complex (i.e. where neutral buoyancy is most probable).

Unfortunately, little is known regarding the nature of the earliest basaltic magmatism, or the overall volume production of such magmas, during the *c*. 2 Ma interval when crustal density structure prevented their eruption. As an indirect means of constraining the scale and energetics of the entire magma system, the remainder of this paper considers the processes required to produce the large volumes of associated rhyolitic magma. It is widely accepted that the energy needed to produce the rhyolites is derived from inputs of basaltic magma into the crust (Lachenbruch *et al.* 1976; Younker & Vogel 1976; Huppert & Sparks 1988; Bergantz 1989; Bittner & Schmeling 1995; Petford & Gallagher 2001; Annen & Sparks 2002; Dufek & Bergantz 2005; Annen *et al.* 2006). Our approach is to consider the volume production, as well as critical physical and chemical properties, of SRPY silicic magmas to constrain physical models for melt generation.

Thermal models for rhyolite generation

Our analysis emphasizes the CSRP rhyolites because their eruptive volumes and temperatures are reasonably well known and their δ^{18}O-depletion provides limits on the possible depth of the rhyolite crustal protolith. Realistic physical models for rhyolite generation are constrained to satisfy the following criteria based on the geologic record and on the geochemical and petrological data. The cumulative amount of CSRP rhyolite ranges from a minimum of 7000 (stratigraphic estimate) to perhaps as much as 30 000 km^3 (tephra estimate coupled with an intrusive:extrusive ratio of 2). Average temperatures above 900 °C are required within the source volumes. Although speculative, it is illustrative to consider the scale of magma production by estimating source volume. Assuming a 50 km radius footprint (i.e. width of the SRP) for the source, and degree of melting near 25%, the above volumes of magma could be produced from cylindrical sources at least 3.6 km thick (these relations and the effect of varying melt fraction, *F*, are illustrated in Fig. 7). Estimates of source thickness may be exaggerated to the extent that an unknown fraction of the overall magma volume is derived from the large basaltic inputs required to drive crustal melting. Even with conservative volume estimates, the scale of the problem is formidable.

The primary purpose of the thermal models presented here is to understand the conditions that can warm such thicknesses of crust to the range of liquidus temperatures estimated for SRPY rhyolites and, in addition, simulate the geologically constrained

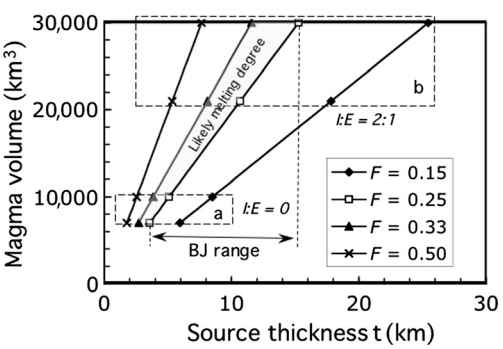

Fig. 7. Diagram showing relation between total magma volume v. thickness of the corresponding source domain as a function of degree of melting or melt fraction (*F*). Source volume is assumed to be cylindrical with a diameter of 100 km (i.e. the width of the SRP). Dashed boxes indicate scenarios based (**a**) solely on erupted volumes ($I{:}E = 0$) and (**b**) on combined eruptive and intrusive volumes ($I{:}E = 2$) for the BJ centre. For $F = 0.25$, source thickness ranges between approximately 3.5 and 15 km to produce limiting volumes (7000–30 000 km^3) of BJ rhyolite. The thickness of the source volume decreases with increasing melt fraction, but even for $F = 0.5$, must exceed at least 2 km.

magma production. We present here the results of one-dimensional heat transfer calculations assuming that melting is driven by repeated injection of hot mafic magmas into the crust. This concept conforms closely with the magma ascent processes discussed earlier.

The computation of heat balance between basaltic intrusions and the surrounding crust takes into account the conductive heat transfer and the latent heat released by crystallization of the basaltic magma:

$$\rho c_p \frac{\partial T}{\partial t} + \rho L \frac{\partial X}{\partial T} = k \frac{\partial^2 T}{\partial x^2} \quad (1)$$

where ρ is density, c_p is specific heat capacity, L is latent heat released by magma crystallization, T is temperature, t is time and x is distance. The equation is solved for the basalt intrusion and country rock systems using forward finite differences. The initial condition is a geotherm of 30 °C km^{-1}. The boundary conditions are a fixed temperature of 0 °C at the Earth's surface and the initial geotherm at depth. More details of the simulation method can be found in Annen *et al.* (2006).

Computation of the latent heat released by crystallization requires knowledge of the relationship between basalt temperatures and melt fractions (Fig. 8). Using MELTS (Ghiorso & Sack 1995; Asimow & Ghiorso 1998), this relationship was modelled for the composition of representative SRP basalt, assumed to contain a small amount (*c*. 0.1 wt%) of H_2O. The effect of increasing H_2O content to 0.4% (typical for many SRP olivine-hosted melt inclusions; C. Stefano, pers. comm.) is also shown in Figure 8; this results in a lowering of temperature by *c*. 50 °C at a given pressure.

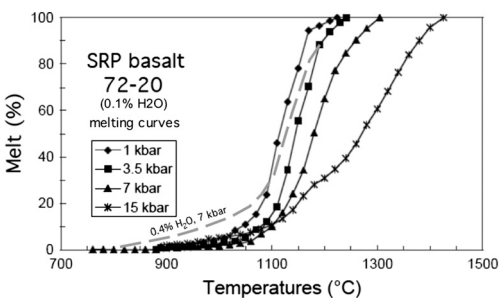

Fig. 8. Relationship between melt fraction and temperature for a SRP primitive basalt (McKinney basalt sample 72-20; Leeman & Vitaliano, 1976) calculated with MELTS at pressures of 1, 3.5, 7 and 15 kbar, FMQ buffer and initial H_2O near 0.1 wt%. Note that water-free solidus temperatures exceed 1050 °C at all pressures. The dashed line shows the effect of increasing H_2O to 0.4% at 7 kbar.

A latent heat of 5.3×10^5 J kg^{-1} was used for the basalt (Kojitani & Akaogi 1994). It should be noted that the small amount of water in this magma results in significant lowering of the solidus at low melt fractions compared with the equivalent dry magma (solidus *T* near 1050 °C).

The composition and melting behaviour of the crustal protolith is not known. For this reason, instead of calculating the melting degree of the crust (which is strongly dependent on assumed bulk composition), we calculated the thickness of crust for which temperature exceeds 900 °C. With this approach, no assumption is required concerning the relationship between temperature and melting degree for the crust. However, because we neglect the latent heat absorbed by crust during partial melting, temperatures are slightly overestimated. We compared the results obtained when neglecting latent heat with results obtained by allowing a granodioritic crust to melt (using the granodiorite melt-temperature relationship as in fig. 1 of Annen & Sparks 2002, granodiorite latent heat of 3.5×10^5 J kg^{-1}, and degree of melting up to 50% at the contact with basalt but decreasing rapidly away from the contact); the maximum error in temperature is 15 °C and the difference in thickness of crust heated above 900 °C is 150 m or less.

We model the emplacement geometry of the growing mafic body by sill over-accretion; i.e. each sill is emplaced above the former one at the top of the mafic body and in contact with the upper crust. This emplacement geometry maximizes temperatures in the shallow crust as well as the degree of crustal partial melting (Annen *et al.* 2008). For convenience, the thickness of individual sills is assumed to be 50 m and models were run with up to 20 km of basalt injected into the crust. Annen & Sparks (2002) show that, as long as the time interval between successive injections is much shorter than the total duration of the simulation, the long-term thermal evolution of the system is independent of the exact thickness of the sills and, rather, depends primarily on the average emplacement rate; this is obtained by dividing the sill thickness by the time interval between sill emplacements.

Repeated infusion of basalt into the crust causes the mafic body to grow and heat the surrounding country rocks, such that temperatures in both the crust and the basalt intrusive complex increase with time. If melt is extracted periodically from the partially molten crust, the residual crust will become more mafic and refractory with time. Also, if crustal partial melts and basalt residual melts reside in the crust for protracted time periods, increasing temperature could result in an increasing melt fraction overall (Annen *et al.*

2006). Both processes are consistent with compositional evolution of the BJ rhyolites, for which SiO_2 content decreases and FeO^T and TiO_2 increase with time.

The evolution of temperature in the crust is controlled by the balance between the heat that is advected by the basalt sills and the heat that is conducted through the crust. The emplacement rate of the basalt controls the distribution of temperature within the crust and its ability to partially melt. We have simulated the repeated injection of basalt sills with different emplacement rates and at different depths over 4 Ma, which is similar to the duration of BJ rhyolitic magmatism. The volume of crust above 900 °C steadily increases with time as long as basalt injection and growth of the composite mafic intrusive complex continue at a sufficient rate (Fig. 9). However, once basalt injection abates or ceases (e.g. due to the source moving along the hot spot track), crustal temperatures and volumes of partial melt begin to decrease. As an example of the timescale for this process, following basalt injection over 4 Ma at a rate of 4 mm year^{-1} (i.e. 16 km of basalt added to the crust), some 1 Ma is required for hot zones in the crust to cool down below 900 °C once basalt input stops.

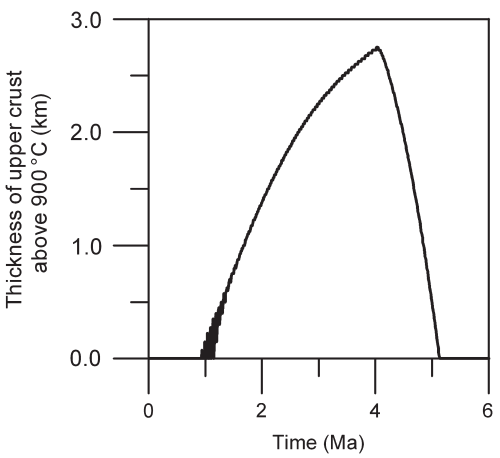

Fig. 9. Temporal evolution of a crustal hot zone. In this model, basalt is repeatedly emplaced at a constant depth of 15 km over 4 Ma with an influx rate of 4 mm year^{-1} (total thickness = 16 km), after which basalt influx terminates and the system begins to cool. The graph illustrates the thickness of upper crust above 900 °C as a function of time; the maximum is less than 3 km for this intrusion rate. In reality, the crust must cool off at a slower pace owing to prolonged basaltic volcanism following the initial pulse of silicic volcanism. Also, note that an incubation period of *c*. 1 Ma is required before a significant volume of crust reaches 900 °C.

The maximum thickness of crust heated above 900 °C increases with increasing basalt emplacement rate and with depth of the mafic body (Fig. 10a & b). If the emplacement rate is less than 2 mm year^{-1}, the crustal temperatures cannot exceed 900 °C on the timescale of 4 Ma except for emplacement depths in the lower crust. Emplacement rates greater than 5 mm year^{-1}, correspond to intrusion of more than 20 km of basalt over 4 Ma, which we consider unlikely (although the upper limit remains unconstrained). To heat more than 2 km of crust above 900 °C, emplacement of a total basalt thickness of at least 12 km is required (equivalent to a minimum basalt intrusion rate of 3 mm year^{-1} over 4 Ma). However, the thickness of basalt that is above 900 °C is at least twice the thickness of old crust heated above 900 °C, and the proportion of basalt becomes greater with increasing emplacement rate (Fig. 10c). The proportion of crust-derived v. basalt-derived melts depends on the relative fertility of these sources. Our results indicate that only with melting degrees of 40% or more (e.g. tonalite source of Patiño-Douce 1997) would the amount of crustal melts exceed the quantity of residual melt generated within the basalt. Despite this, the dominantly crustal geochemical signature of voluminous early BJ rhyolites suggests that, during this stage, crustal-derived melts were preferentially extracted with only moderate dilution by residual basalt-derived liquids. Conversely, during the waning later stage, contributions from residual basaltic liquids increased in proportion.

Our thermal model is not dynamic and the withdrawal and eruption of melt is not explicitly simulated. Although Jackson *et al.* (2003) showed that melt composition evolves during compaction, our knowledge of the system and of the physical parameters that control its dynamic behaviour is insufficient to warrant complex simulations that include compaction, extraction and possibly injection at shallower depths. Extraction of melt will not modify the temperature of the rock from which it was removed but transfer or reinjection of such melts elsewhere within the crustal hot zone could alter the temperature profile in the melting zone. This process is unlikely to significantly affect the thicknesses of heated crust (shown in Figs 9 & 10) as long as the volume of mobile melt involved is small compared with the volume of solid heated rocks.

In our model system, where mafic magma is incrementally emplaced as sill intrusions, each successive sill cools down on time scales of a few hundreds to a few thousand years depending on its exact thickness (figs 7 and 19 of Annen *et al.* 2006). Following thermal equilibration with the surrounding wall rocks, temperatures of the intrusions,

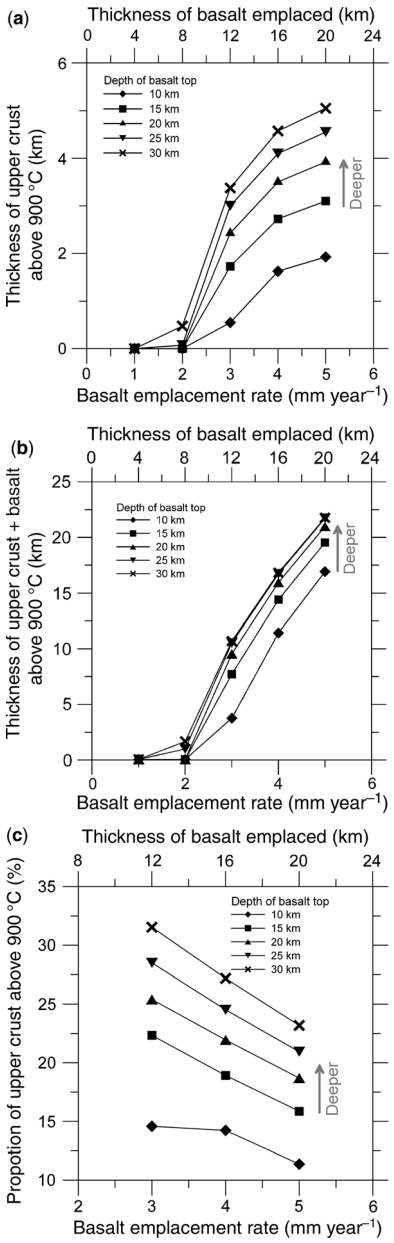

Fig. 10. Thickness of upper crust and basalt with temperatures above 900 °C after 4 Ma of repeated basalt emplacement as functions of mafic magma emplacement rate (i.e. total thickness of emplaced basalt) and emplacement depth. Magma emplacement at depths shallower than 5 km, even at high emplacement rate, cannot bring the crustal wall rocks to 900 °C. (**a**) Thickness of pre-existing upper crust heated to $T \geq 900$ °C. (**b**) Thickness of basalt plus old upper crust heated to $T \geq 900$ °C. (**c**) Percentage of old upper crust heated above 900 °C relative to the total (upper crust + basalt) that is above 900 °C.

hence also compositions of the residual melts, evolve slowly as the whole system progressively warms up. Mafic and possibly intermediate composition melts are probably preserved in late-injected sills that had insufficient time to equilibrate with the remaining crust. Because of the thermal gradient within the basalt and intruded crust, spatial diversity in melting degree and in melt composition is predicted. For anhydrous basaltic intrusions, the maximum model temperature (*c*. 1140 °C) corresponds to a melt fraction of less than 0.25, which is likely to have a relatively silicic composition. For more hydrous basalt (cf. Fig. 8), melting degrees would be higher at comparable temperatures and liquids of intermediate composition would be produced.

The volume of melt produced can be scaled to match BJ eruptive volumes. Figure 11 shows the predicted evolution of the temperature distribution within the crust when basalt sills are emplaced at an average rate of 4 mm year^{-1}. After 4 Ma, this scenario results in heating a volume of crust (*c*. 2.8 km thick) that is insufficient to match the minimal BJ extrusive volume (7000 km^3) if the rhyolites are pure crustal melts and F smaller than 0.33. To heat the necessary thickness of crust (3.6 km for $F = 0.25$) requires longer time of intrusion (i.e. longer incubation time), higher basalt input rate or a combination of these factors. To produce greater (and more realistic) total melt volumes (>10 000 km^3) strictly from the crust requires even more extreme adjustments of one or more of these parameters and/or, greater lateral dimension of the source volume. Within limits provided by geochemical constraints, the total volume of magma in the system could also be enhanced by liquids produced by differentiation of the intruded basalt or remelting of portions of the mafic intrusive complex. For the BJ centre basalt-derived melt contributions are inferred to increase as the system evolved and became warmer in response to progressive intrusion of basaltic magma into the shallow crust.

Our modelling suggests that a composite mafic body less than 20 km thick, emplaced over intervals of 2–4 Ma, can elevate temperatures above 900 °C within only a few kilometres of proximal pre-existing crust (Fig. 10a), particularly if intrusion depths are shallower than 20 km. It is difficult to maintain such high temperatures at depths shallower than 5–10 km owing to initially low wall rock temperatures and considerable heat losses to the surface. We also note that relatively fertile source rocks considered previously by Annen and coworkers are not well suited as protoliths in this setting because they produce a considerable amount of melt at temperatures well below those of SRPY silicic magmas, and

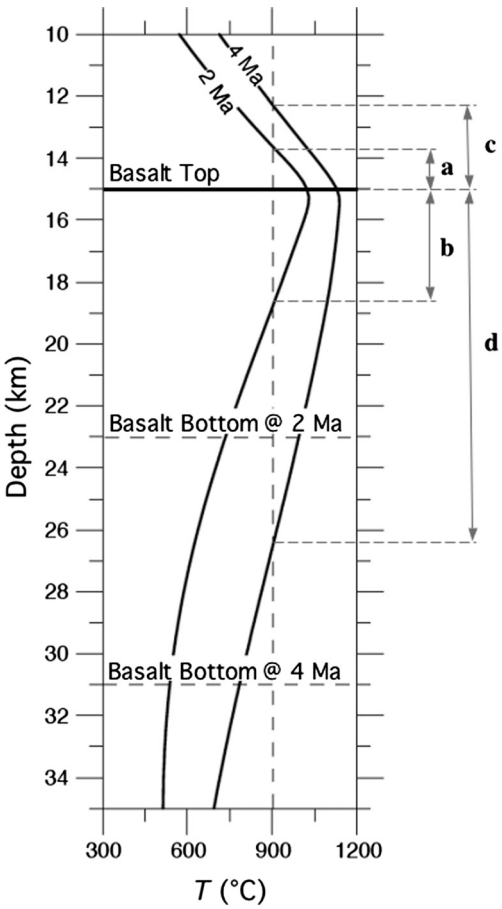

Fig. 11. Profiles of temperature v. depth in the crust after 2 and 4 Ma of basalt emplacement at a sustained rate of 4 mm year^{-1} In this model, successive basalt sills are emplaced at 15 km depth. Over this time interval, the thickness of a crustal hot zone ($T > 900$ °C) varies from about 4.5 to 14 km. Note: **a** and **b** are thicknesses of upper crust and intruded basalt heated above 900 °C after 2 Ma; **c** and **d** are thicknesses of upper crust and intruded basalt heated above 900 °C after 4 Ma.

there is no surface manifestation of such magmatism.

Assuming that depths of pervasive ^{18}O-depletion are probably restricted to the uppermost portions of the crust, and that such modified rocks are protoliths for the BJ rhyolites, it appears inescapable that sizable mafic intrusions must be concentrated in the shallow crust (probably within 15 km of the surface) to promote extensive melting of these distinctive domains. For such conditions our models for the BJ magmatic system require a larger addition (*c.* 16 km thickness over 4 Ma) of basaltic magma to the crust. This new estimate is about twice that based only on a simple energy balance (*c.* 8–10 km over 4 Ma; Bonnichsen *et al.* 2008). This difference reflects the fact that the latter approach ignores substantial dissipation and refraction losses of heat associated with incremental intrusion of basalt. For a circular footprint with 100 km diameter, the time-averaged basalt flux is between 0.024 and 0.031 km^{3}year^{-1}; i.e. about an order of magnitude smaller than the magma flux for Kilauea volcano (*c.* 0.2 km^{3}year^{-1}; Crisp 1984).

Oxygen isotopic constraints on rhyolite genesis

The oxygen isotope problem

Because of its importance in constraining melting depths in the crust, we now return to the issue of how ^{18}O-depletion in the BJ rhyolite source could be related to infiltration of waters controlled by near surface processes preceding and possibly attending magmatism in the region. It is well known that hydrothermal circulation can lead to chemical and isotopic alteration of aureoles surrounding epizonal plutons, but it is not clear how deep such effects can extend or to what extent O isotopic compositions of crustal rocks can be shifted as a function of depth. It is clear that modest ^{18}O-depletion extends to magma chamber depths in many places. Bindeman *et al.* (2004) present extensive data for Kamchatka suggesting that ^{18}O-depletion is related to deep circulation of meteoric waters, and suggest that magnitude of the ^{18}O-shift depends on latitude and climate influences on water compositions. Moreover, these authors show that ^{18}O-depletion is more pronounced in caldera-related silicic magmas than in smaller stratovolcanoes. The difference could be related to tectonic and structural controls that influence fluid circulation, leading to heterogeneous crustal modification. These are critical issues in understanding origins of SRPY silicic magmas.

Given the outcomes of our thermal models, it seems virtually impossible to get crustal temperatures above 900 °C at depths shallower than 5–10 km for volumes of crust approaching even the minimum estimate for the rhyolite source. This implies that fluid infiltration and significant O-exchange must reach greater depths to explain the chemistry of BJ rhyolites. If this condition was established in the crust prior to the earliest BJ eruptions, the modification could have occurred over a relatively long time period; it could also have been a partly syn-magmatic process. We consider the 'open ended' questions: given unlimited time, and that Miocene precipitation in the

region had $\delta^{18}O$ near −20‰ (cf. Hearn *et al*. 1989; Horton *et al.* 2004), what is the maximum lowering of $\delta^{18}O$ that can be achieved in the crust and how deep could the modification extend? Specifically, can this process realistically create large volumes of crustal rocks (e.g. a 100 km diameter cylindrical disk at least 3.6 km thick) with $\delta^{18}O$ in the range observed in BJ rhyolites, and at appropriate depths where thermal conditions are suitable for generation of silicic magmas in volumes matching the estimated magmatic outputs? And, assuming that the underlying crust started with normal $\delta^{18}O$ (*c*. 10‰), what processes and/or conditions are required to modify the magma source to values as low as −2‰?

Theoretical considerations

The rate of ^{18}O-depletion of the crust is controlled by both the supply of low $\delta^{18}O$ meteoric waters at depth and by the kinetics of either oxygen exchange between the water and the permeable crystal framework or growth of new phases. The kinetics of oxygen exchange is highly dependent on the temperature of the reaction. A detailed calculation of the kinetics of the oxygen exchange process in porous media will be presented elsewhere, but insight can be gained from the observation that oxygen diffusivity drops four orders of magnitude between 800 and 400 °C in plagioclase (from *c*. 1×10^{-16} to 1×10^{-20} $m^2\ s^{-1}$) and is more than 10 orders of magnitude less than the equivalent thermal diffusivities (Cole & Ohmoto 1986). However, provided the crust is sufficiently permeable, advection of hydrothermal waters allows diffusion to operate at the grain-scale.

The thermal gradient in the crust can be combined with a grain-diffusion model and appropriate temperature dependent oxygen diffusivities and fractionation factors to estimate the maximum possible $\delta^{18}O$ depletion in the crust. We also consider an end member in which separate phases have reached equilibrium with the circulating hydrothermal waters; this end member can also be thought of as a proxy for new phases that may grow in the presence of the hydrothermal waters. In these calculations we implicitly assume that the fluid $\delta^{18}O$ is constant and equivalent to −13‰, a median value for $\delta^{18}O$ measured in geothermal waters in southwestern Idaho (Rightmire *et al.* 1976). We use a $\delta^{18}O$ higher than the meteoric value (*c*. −20‰) because, at depth, the composition of water percolating through regions of low flux likely will be altered by oxygen exchange with crustal rocks. Values of $\delta^{18}O$ even greater than −13‰ are likely at depth as the measured surface geothermal fluids probably contain a component of near surface, unaltered water (Allan & Yardley 2007). Hence the following calculations should be viewed as indicating maximum depletions.

In delta notation, an adapted analytical expression for diffusion in a spherical grain is given as (Carslaw & Jaeger 1959):

$$\frac{\delta^{18}O_r(r,t) - \delta^{18}O_r^0}{\delta^{18}O_r^B - \delta^{18}O_r^0} = 1 + \frac{2a}{\pi r}\sum_{n=1}^{\infty}\frac{-1^n}{n}\sin\left(\frac{\pi n r}{a}\right)\exp\left(\frac{\pi^2 n^2 D t}{a^2}\right). \quad (2)$$

Here and below, a denotes the crystal radius, r is the radial distance, D is the diffusivity, $\delta^{18}O_r^0$ is the initial rock composition (taken as 10‰), $\delta^{18}O_w^0$ is the water composition (taken as −13 ‰), $\delta^{18}O_r(r, t)$ is the time and radially dependent $\delta^{18}O$ in the mineral, t is time, n is the dummy variable for the summation calculation, and $\delta^{18}O_r^B$ is the mineral equilibrium composition at the grain boundary. The grain boundary condition here is given as a function of the water composition, the equilibrium fractionation factor, and the mass and composition of water and rock.

$$\delta^{18}O_r^B = -\Delta_{w-r} + \delta^{18}O_w^0 + \left(-\delta^{18}O_w^0 + \Delta_{w-r} + \delta^{18}O_r^0\right) \times \exp\left[\frac{-c_W m_W}{c_R m_R}\right]. \quad (3)$$

Here m_W and m_R are the mass of water and rock, respectively, and c_W and c_R are the elemental concentrations of oxygen in water and rock, and Δ_{w-r} (T) is the temperature dependent equilibrium fractionation factor. Note that if the flux of water is high (the mass of water to rock approaches infinity), the grain boundary composition approaches the equilibrium value of:

$$\delta^{18}O_r^B = \delta^{18}O_w^i - \Delta_{w-r.} \quad (4)$$

If the flux of water is limited at the grain boundary due the permeability of the matrix, the boundary will be modified by the exponential term in Equation 3. Ingebritsen & Manning (1999) suggest a permeability profile based on geothermal and fluid flux data:

$$k = 10^{-14-3.2\log^z} \quad (5)$$

where z is in kilometres. Near the brittle – ductile transition, fluid pressures may become greater than hydrostatic pressure, inhibiting the deeper circulation of water at depth (Huenges *et al.* 1997; Brown 2007). Although this transition probably

Table 2. *Diffusivity and fractionation factor coefficients*

Mineral	A	B	C	A_0 ($m^2\ s^{-1}$)	E_a ($J\ mol^{-1}$)
Anorthite	4.12	−7.5	2.24	1.39×10^{-11}	109,600
Albite	4.33	−6.15	1.98	9.8×10^{-10}	139,800
K-Feldspar	4.32	−6.27	2.0	3.95×10^{-12}	109,700
Quartz	4.48	−4.77	1.71	2×10^{-9}	184,000
Hornblende	3.89	−8.56	2.43	1×10^{-11}	171,600
Biotite	3.84	−8.76	2.46	9.1×10^{-10}	142,300

Equilibrium fractionation factor coefficients (used in Equation 7) are from Zheng (1993*a*, *b*). The diffusion coefficients for the specific phases (used in Equation 8) are from experiments (Giletti *et al.* 1978; Yund *et al.* 1981; Giletti & Yund, 1984; Farver & Giletti, 1985; Cole & Ohmoto, 1986; Fortier & Giletti, 1991; Freer *et al.* 1997; Cole & Chakraborty, 2001).

occurs over a range of temperatures depending on the lithology, we use 400 °C as the transition where the crystalline rock becomes ductile over long timescales (Manning & Ingebritsen 1999).

The mass of water that passes through a unit volume of rock is then:

$$m_W = q \cdot t = -\frac{10^{-14-3.2\log z}}{\mu_{water}} \frac{\partial[\Delta\rho_{water} g z]}{\partial z} \cdot t. \quad (6)$$

Here q is the water flux, μ_{water} is the water viscosity, ρ is density, and g is the gravitational acceleration. The equilibrium fractionation factors (in Δ notation where $\Delta_{w-r} = 10^3 \ln \alpha$, and α is the equilibrium fractionation water-rock ratio) are given as

$$\Delta = \frac{A \times 10^6}{T^2} + \frac{B \times 10^3}{T} + C \quad (7)$$

where A, B, C for the specific mineral phases are taken from Zheng (1993*a*, *b*; cf. Table 2). Oxygen diffusivities for specific phases are calculated from an Arrhenius expression,

$$D = A_0 \exp\left[\frac{E_a}{RT}\right] \quad (8)$$

where the pre-exponential (A_0) and activation energy E_a terms are calibrated from appropriate experiments (cf. Table 2).

Solving Equation 2 for $\delta^{18}O_r(r, t)$, performing the spherical integration and dividing by the volume gives the mean oxygen isotopic composition, $\delta^{18}\bar{O}_r(t)$, of crystals that we take as a proxy for the crust at a particular time and depth. Assuming a geothermal gradient of 25 °C km^{-1}, 2.5 mm crystal radii, and using Equations 2–8 gives depth-composition profiles for feldspars, quartz, hornblende and biotite after 1 Ma of interaction (Fig. 12). Profiles are shown for two extreme scenarios assuming either 'infinite' access of fluid (i.e. very large water–rock ratios), or a more realistic water-flux limited case wherein fluid flow is governed by Darcy's law, the permeability given in Equation 5, and a lithostatic pressure gradient. In the second case, if permeability *was* substantially enhanced, the profiles in Figure 12c would approach but never exceed those in Figure 12b. We again note that these profiles represent maximum depletions as we assume a constant fluid composition.

A second scenario is considered in which a thermal anomaly from prior intrusions has warmed the mid-upper crust (Fig. 13a). Similar oxygen depletion calculations are performed for this thermal condition. The maximum depletion profiles (Fig. 13b) have proceeded to equilibrium with the circulating water. This end member can also be thought of as a proxy for recrystallizing phases in the presence of the hydrothermal fluid. The minimum depletion calculation is constrained by the amount of water that passes through the permeable rock (Fig. 13c). Although degrees of ^{18}O-depletion are similar for both scenarios, the maximum depletion is shifted to shallower depths and the thickness of the zone of depletion is also diminished for warmer crust.

The assumption of a constant boundary condition of meteoric water $\delta^{18}O$ breaks down where permeability significantly reduces the fluid flux. Although temperature increases with depth in the crust, the reduction in mean permeability limits the degree of oxygen exchange (Manning 1981). In general, $\delta^{18}O$ depletion in the upper crust is kinetically (thermally) limited, and $\delta^{18}O$ depletion in the deep crust is water flux (permeability) limited.

Finally, we note that isotopic shifts are more pronounced for feldspars and biotite than for quartz or hornblende. Thus, ^{18}O-depletion for the bulk crust will depend on lithology and mineral proportions. The oxygen isotopic composition of crustal melts could then differ depending on specific lithologies and oxygen exchange histories of their source rocks.

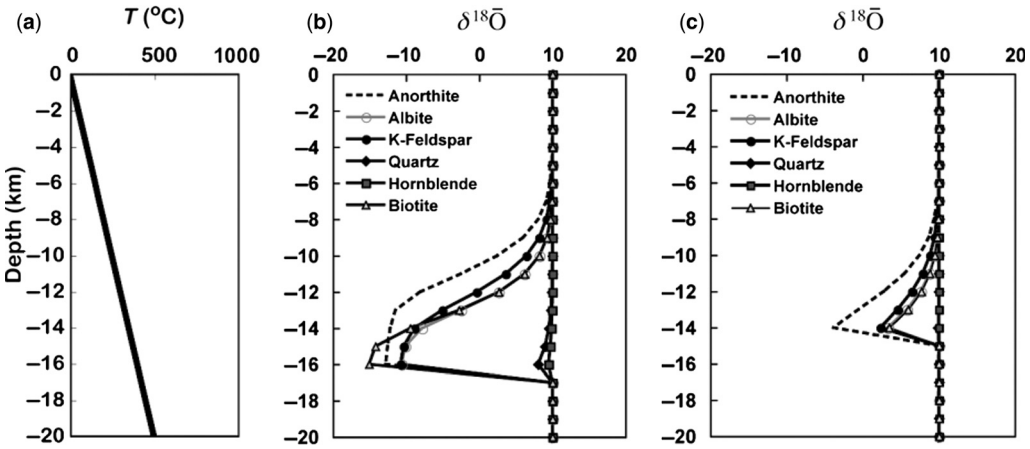

Fig. 12. Calculated effects of infiltrating surface waters on oxygen isotopic composition of crustal minerals as a function of depth. Models include temperature-dependent diffusion kinetics and isotopic fractionation effects and assume input of constant composition of meteoric water; see text for details. Two scenarios are presented, both for 1 Ma time interval: (**a**) shows the thermal profile used in this calculation; (**b**) shows the effect of having an infinite supply of surface fluid, but with fluid circulation inhibited at the transition to ductile crust; (**c**) incorporates permeability-limited fluid infiltration using the permeability – depth relation of Ingebritsen & Manning (1999), and is considered more realistic for diffusional exchange. In both cases, kinetic effects associated with lower temperatures limit isotopic exchange at shallow crustal depths. These models, and (**c**) in particular, suggest that ^{18}O-depletion varies with depth and may display a maximum effect in a specific depth range – in this case, near 15 km.

Results

The first order result of these models is that ^{18}O-depletion in the shallow to mid crust appears to be of sufficient magnitude to match that required for the BJ rhyolite source volume (i.e. δ^{18}O as low as -2‰). Maximum effects are localized in the depth range between 10 and 15 km depending on crustal lithology. Our models for thermally perturbed syn-magmatic crust essentially limit

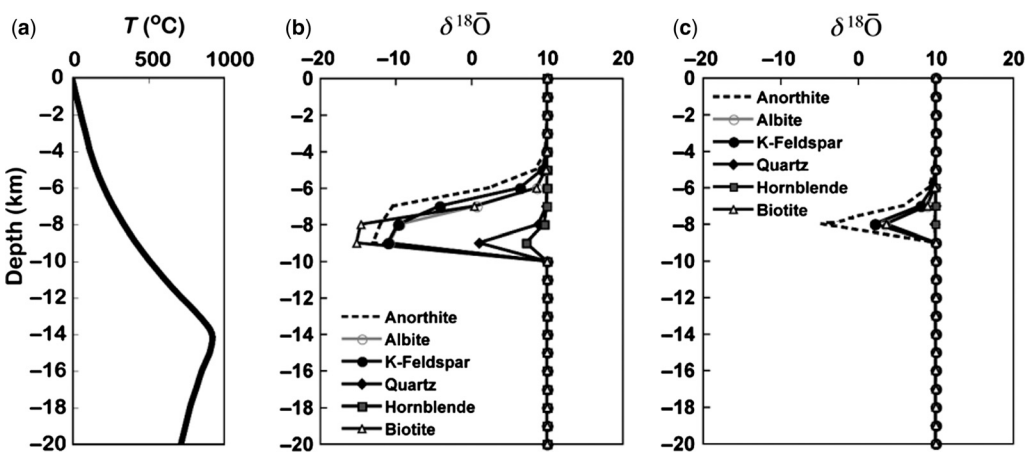

Fig. 13. Calculated effects of infiltrating surface waters on oxygen isotopic composition of crustal minerals as a function of depth, as in previous figure but with a syn-volcanic scenario in which the geothermal gradient is perturbed by repeated magma injections. Again, two scenarios are presented, both for 1 Ma time interval: (**a**) shows the perturbed thermal profile used; (**b**) shows effect of having an infinite supply of water, and profiles indicate maximum δ^{18}O-depletion for diffusion exchange or recrystallization; (**c**) incorporates permeability-limited fluid infiltration. In both cases, we assume that fluid pressures exceed hydrostatic pressure and inhibit circulation of meteoric waters at depths below the brittle – ductile transition (i.e. at temperatures above 400 °C).

^{18}O-depletion to depths shallower than 10 km where it is extremely difficult to heat significant volumes of crust to 900 °C or more. This result is consistent with the notion that crustal modification largely predated onset of CSRP magmatism. The fact that early rhyolites from the Heise and Yellowstone volcanic fields have 'normal' δ^{18}O implies that meteoric fluids did not significantly modify their source rocks.

Discussion and summary

This work provides new insights into the origin of silicic magmas associated with the Yellowstone melting anomaly. Observations of CSRP rhyolites provide critical constraints on the melting processes by which they formed. Foremost are the large magma volumes, the consistently elevated magmatic temperatures, the long duration of silicic magmatism, and the bimodal basalt – rhyolite productivity (with sparse intermediate composition magmas). Also, the transition from dominantly silicic to dominantly basaltic volcanism over time provides insight regarding the influence of the continental crust on magmatic processes (and vice versa).

Our interpretation of how SRPY magmatism affected the underlying crust is summarized in Figure 14. We view CSRP silicic magmatism as being broadly representative of that for the entire province. However, owing to diachronous development, the Yellowstone volcanic centre presently is at a relatively early evolutionary stage compared with older centres to the west that have essentially run their course in terms of silicic volcanism. Furthermore, lateral or vertical heterogeneities in the underlying crust may impose important differences in magmatic response across the province. For example, ^{18}O-depletion in crustal sources appears to be more extensive beneath the CSRP, and suggests that fluid-related alteration of the crust was more extensive in that area. The unusual temporal variation in composition of BJ rhyolites, that is both highly systematic yet opposite from normal magmatic differentiation trends, also implies that melting processes varied in detail across the province. Key findings from this study are highlighted below.

Combined constraints of thermal modelling and oxygen isotopic evidence for an ^{18}O-depleted source strongly limit depths of magma formation in the CSRP. The latter observation provides compelling evidence that these rhyolites were predominantly crustal melts because (a) low-δ^{18}O is unlikely to be inherited from the mantle and (b) oxygen comprises more than 50% of the magma by weight. The strongly bimodal (basalt – rhyolite) compositions of erupted magmas, and the restricted compositional range for the rhyolites, suggest that direct mixing between basaltic magma and silicic crustal melts is limited ($<c.$ 10%, based on mass balance considerations). Relatively radiogenic Nd compositions of BJ rhyolites preclude wholesale melting of old crust, and are consistent with contributions of evolved liquids of basalt-derivation (e.g. by differentiation or remelting) to direct crustal melts; such contributions appear to be

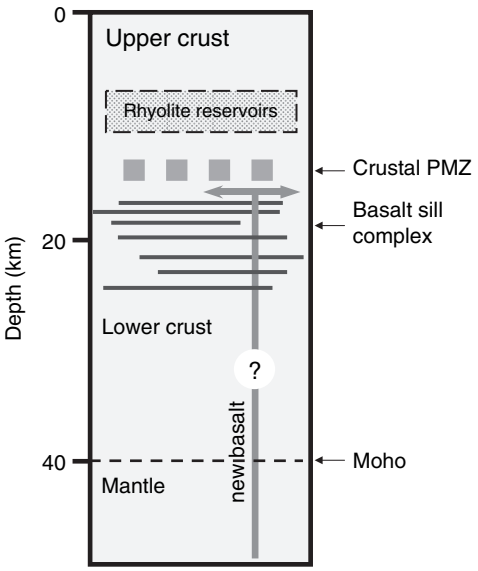

Fig. 14. Schematic diagram for crust beneath the CSRP. Major injections of basalt occur at depths as shallow as *c.* 15 km by an overaccretion process that results in downward displacement of the intrusive sill complex. Rhyolite generation occurs largely in a crustal partial melt zone (PMZ) above the sill complex and may be augmented by incorporation of remobilized evolved melts derived from the basaltic sills (via normal differentiation and/or remelting of intrusive equivalents). Prior to eruption, rhyolitic magmas may coalesce in a plexus of shallow reservoir lenses as inferred for Yellowstone. The crustal section must deform to accommodate the volume of basaltic intrusions, either by extension or some form of crustal flow. It is suggested that attenuation of the crust is approximately balanced by new basaltic inputs so as to maintain near-constant crustal thickness. We assume that such a configuration extends beneath most of the SRPY province, and that peak basaltic intrusion into the crust migrated northeastward with time as reflected by migration of silicic volcanic centres in Figure 1. However, continued basaltic inputs sustained the thermal anomaly and locally led to renewed silicic magmatism (McCurry *et al.* 2007). Basaltic inputs to the deep crust remain uncertain, but no erupted lavas are thought to originate from such depths.

more substantial (perhaps up to 50%) in the younger rhyolite lavas than in the early ignimbrites (<20%).

Owing to decreasing permeability with depth, it is difficult to produce an ^{18}O-depleted crustal volume capable of generating the estimated volume of CSRP rhyolites. Assuming optimal conditions, theoretical simulations of downward circulation of surficial fluids suggest that maximum ^{18}O-depletion is likely to be concentrated at depths near 15 km for a normal crustal geotherm (*c*. 25 °C km^{-1}), but as shallow as 8–10 km for warmer, syn-magmatic geotherms. The latter scenario is least favoured owing to (a) the difficulty in reaching crustal melting conditions at such shallow depths, and (b) the fact that ^{18}O-depletion must have largely predated the earliest (12.7 Ma) BJ silicic volcanism. Causes for the crustal modification remain uncertain. In addition to processes suggested by Boroughs *et al.* (2005), access of sufficient fluid to produce the required volume of low-δ^{18}O crust may require enhanced fluid permeability due to crustal deformation. Also, the inferred source area for the most ^{18}O-depleted BJ rhyolites roughly coincides with the presence of a large lacustrine environment (Lake Idaho) in topographically low parts of the west-central SRP during Neogene time (fig. 1 of Beranek *et al.* 2006); thus, proximity of lake waters might have enhanced fluid infiltration and ^{18}O-depletion of the underlying crust. Control by such factors as well as heterogeneous crustal permeability could possibly account for variable ^{18}O-depletion in rhyolite magmas from the CSRP.

Our thermal models indicate that a large volume of basalt (equivalent to a thickness as great as 16 km) must be injected incrementally into the crust over a period of several Ma to raise temperatures to those of the rhyolite magmas (≥900 °C) within a thickness of crust large enough to generate the estimated volume of CSRP rhyolitic magmas. It is increasingly difficult to achieve this condition as depth of basaltic intrusion decreases, and virtually impossible at depths shallower than 5–10 km. Because these results are predicated on minimal to modest estimates of source volume thickness, the amounts of intruded basalt could be larger.

In summary, the 'sweet spot' for magma generation that ideally satisfies both the thermal and oxygen isotope constraints appears to centre near a depth of 15 km. Partial melting of crustal rocks near this depth can satisfy experimental constraints that A-type magmas probably form at low pressures (*c*. 4 kbar). Intrusion and storage of basaltic magmas at this depth can also explain the persistent occurrence of a low-pressure phenocryst assemblage and absence of clinopyroxene in erupted SRPY basalts. Emplacement of large volumes of basalt into the crust inevitably leads to a preponderance of this material relative to the thickness of pre-existing crust that will remain for long times at temperatures above 900 °C.

Given that crustal thickness is nearly uniform (*c*. 40 km) beneath the entire province, it appears that added volumes of basalt must somehow be accommodated by extensional deformation of the crust and lithosphere (Rodgers *et al.* 2002; Wood & Clemens 2002). Bonnichsen *et al.* (2008) present a simple two-dimensional model using geologically constrained extension rates (2–3% Ma; Rodgers *et al.* 2002) wherein predicted attenuation and thickening by basalt intrusion combine to maintain near-constant crustal thickness. The higher flux estimates from our study exacerbate the 'room problem' and seemingly require more dramatic extension along the province. A time-averaged extension rate near 5%/Ma could accommodate the upwardly revised basalt influx while still preserving a constant crustal thickness, but at present there is little quantitative evidence for this amount of extension. Thus, we believe that true basaltic flux for the SRPY province is unlikely to be larger than the maximum considered in this study, i.e. about one-tenth that estimated for Kilauea volcano.

Further work is required to better understand the history of crustal deformation, its relation to regional Basin and Range extension, and how the predicted large volumes of basalt can be accommodated within the crust. Crustal deformation may not have been uniform in space or time, and could have been more extensive in the CSRP than in the eastern part of the province. Although there is evidence for development of a deformation parabola ahead of the migrating Yellowstone hotspot (cf. Pierce & Morgan 1991), there is only limited evidence for syn-volcanic extensional deformation of the SRP and its margins (cf. Bonnichsen *et al.* 2007).

Finally, based on the respective eruptive volumes of rhyolite, apparent basalt flux for the BJ volcanic centre is seemingly higher than that for the Yellowstone area. In both cases, the inferred basalt flux is significantly lower than that estimated for Hawaii – thus, raising doubt as to whether SRPY magmatism is dominantly hotspot-driven. Given the evidence for concurrent lithospheric extension, it is possible that widespread basaltic magmatism associated with the province could be related in part to extensional tectonism. Better understanding of lateral variations in the basalt flux is needed to evaluate underlying causes for SRPY magmatism.

The author acknowledges support from the National Science Foundation in the form of research grants and for the time spent on this research since moving to NSF. Dufek acknowledges support from the Miller Institute,

University of California, Berkeley. We also thank D. Geist, J. L. Vigneresse, and M. Jackson for helpful reviews and G. Zellmer for editorial suggestions that greatly improved our presentation.

References

ALLAN, M. N. & YARDLEY, B. W. D. 2007. Tracking meteoric infiltration into a magmatic – hydrothermal system: a cathodoluminescence, oxygen isotope and trace element study of quartz from Mt. Leyshon, Australia, *Chemical Geology*, **240**, 343–360.

ANNEN, C. & SPARKS, R. S. J. 2002. Effects of repetitive emplacement of basaltic intrusions on thermal evolution and melt generation in the crust. *Earth and Planetary Science Letters*, **203**, 937–955.

ANNEN, C., BLUNDY, J. D. & SPARKS, R. S. J. 2006. The genesis of calcalkaline intermediate and silicic magmas in deep crustal hot zones. *Journal of Petrology*, **47**, 505–539, DOI: 10.1093/petrology/egi084.

ANNEN, C., BLUNDY, J. & SPARKS, R. S. J. 2008. The sources of granitic melt in deep hot zones. *Transactions of the Royal Society of Edinburgh* (in press).

ARMSTRONG, R. L., LEEMAN, W. P. & MALDE, H. E. 1975. K–Ar dating of Quaternary and Neogene volcanic rocks of the Snake River Plain, Idaho. *American Journal of Science*, **275**, 225–251.

ASIMOW, P. D. & GHIORSO, M. S. 1998. Algorithmic modifications extending MELTS to calculate subsolidus phase relations. *American Mineralogist*, **83**, 1127–1132.

BALSLEY, S. D. & GREGORY, R. J. 1998. Low-$\delta^{18}O$ silicic magmas: Why are they so rare? *Earth and Planetary Science Letters*, **162**, 123–136.

BERANEK, L. B., LINK, P. K. & FANNING, C. M. 2006. Miocene to Holocene landscape evolution of the western Snake River Plain region, Idaho: using the SHRIMP detrital zircon provenance record to track eastward migration of the Yellowstone hotspot. *Geological Society of America Bulletin*, **118**, 1027–1050.

BERGANTZ, G. W. 1989. Underplating and partial melting: implications for melt generation and extraction. *Science*, **245**, 1093–1095.

BINDEMAN, I. N. & VALLEY, J. W. 2001*a*. Low-$\delta^{18}O$ rhyolites from Yellowstone: magmatic evolution based on analyses of zircons and individual phenocrysts. *Journal of Petrology*, **42**, 1491–1517.

BINDEMAN, I. N. & VALLEY, J. W. 2001*b*. Post-caldera volcanism: In situ measurement of U-Pb age and oxygen isotope ratio in Pleistocene zircons from Yellowstone caldera. *Earth and Planetary Science Letters*, **189**, 197–206.

BINDEMAN, I. N., PONOMAREVA, V. V., BAILEY, J. C. & VALLEY, J. W. 2004. Volcanic arc of Kamchatka: A province with high-$\delta^{18}O$ magma sources and large-scale $^{18}O/^{16}O$ depletion of the upper crust. *Geochimica et Cosmochimica Acta*, **68**, 841–865.

BINDEMAN, I. N., WATTS, K. E., SCHMITT, A. K., MORGAN, L. A. & SHANKS, P. W. C. 2007. Voluminous low d18O magmas in the late Miocene Heise volcanic field, Idaho: implications for the fate of Yellowstone hotspot calderas. *Geology*, **35**, 1019–1022, DOI: 10:1130/G24141A.1.

BITTNER, D. & SCHMELING, H. 1995. Numerical modeling of melting processes and induced diapirisms in the lower crust. *Geophysical Journal International*, **123**, 59–70.

BONNICHSEN, B., LEEMAN, W. P., HONJO, N., MCINTOSH, W. C. & GODCHAUX, M. M. 2008. Miocene silicic volcanism in southwestern Idaho: Geochronology, geochemistry, and evolution of the central Snake River Plain. *Bulletin of Volcanology*, **70**, 315–342, DOI: 10.1007/s00445-007-0141-6.

BOROUGHS, S., WOLFF, J., BONNICHSEN, B., GODCHAUX, M. & LARSON, P. 2005. Large volume, low-$\delta^{18}O$ rhyolites of the central Snake River Plain, Idaho, USA. *Geology*, **33**, 821–824.

BROWN, M. 2007. Crustal melting and melt extraction, ascent and emplacement in orogens: mechanisms and consequences. *Journal of the Geological Society of London*, **164**, 709–730.

CARSLAW, H. S. & JAEGER, J. C. 1959. *Conduction of Heat in Solids*. Clarendon Press, Oxford.

CATHEY, H. E. & NASH, B. P. 2004. The Cougar Point Tuff: Implications for thermochemical zonation and longevity of high-temperature, large-volume silicic magmas of the Miocene Yellowstone hotspot. *Journal of Petrology*, **45**, 27–58.

CATHEY, H. E., NASH, B. P., VALLEY, J. W., KITA, N., USHIKUBO, T. & SPICUZZA, M. 2007. Pervasive and persistent large-volume, low delta 18O silicic magma generation at the Yellowstone hotspot, 12.7–10.5 Ma: Ion microprobe analyses of zircon in the Cougar Point Tuff. *Transactions of American Geophysical Union*, **88**, V51C-0708.

CHRISTIANSEN, E. H. & MCCURRY, M. 2008. Contrasting origins of Cenozoic silicic volcanic rocks from the western Cordillera of the United States. *Bulletin of Volcanology*, **70**, 251–267, DOI: 10.1007/s00445-007-0138-1.

CHRISTIANSEN, R. L. 2001. *The Quaternary and Pliocene Yellowstone Plateau Volcanic Field of Wyoming, Idaho, and Montana*. US Geological Survey Professional Papers, **729-G**, 1–145.

COLE, D. R. & CHAKRABORTY, S. 2001. Rates and mechanisms of isotopic exchange. *Reviews in Mineralogy and Geochemistry*, **43**, 83–223.

COLE, D. R. & OHMOTO, H. 1986. Kinetics of isotopic exchange at elevated temperatures and pressures. *Reviews in Mineralogy and Geochemistry*, **16**, 41–90.

CRISP, J. A. 1984. Rates of magma emplacements and volcanic output. *Journal of Volcanology and Geothermal Research*, **20**, 177–211.

CRISS, R. E. & FLECK, R. 1987. *Petrogenesis, Geochronology, and Hydrothermal Systems of the Northern Idaho Batholith and Adjacent Areas Based on $^{18}O/^{16}O$, D/H, $^{87}Sr/^{86}Sr$, K–Ar, and $^{40}Ar–^{39}Ar$ studies*. US Geological Survey Professional Papers, **1436**, 95–137.

DOE, B. R., LEEMAN, W. P., CHRISTIANSEN, R. L. & HEDGE, C. E. 1982. Lead and strontium isotopes and related trace elements as genetic tracers in the Upper Cenozoic rhyolite-basalt association of the Yellowstone Plateau volcanic field. *Journal of Geophysical Research*, **87**, 4785–4806.

DUEKER, K., STACHNIK, J., YUAN, H. & SCHUTT, D. 2007. Image of Yellowstone magmatic history and

lower crustal outflow. *Abstracts with Programs, Geological Society of America*, **39**, 202.

DUFEK, J. & BERGANTZ, G. W. 2005. Lower crustal magma genesis and preservation: a stochastic framework for the evaluation of basalt-crust interaction. *Journal of Petrology*, **46**, 2167–2195.

EATON, G. P., CHRISTIANSEN, R. L., IYER, H. M., MABEY, D. R., BLANK, H. R., ZIETZ, I. & GETTINGS, M. E. 1975. Magma beneath Yellowstone National Park. *Science*, **188**, 787–796.

FARVER, J. R. & GILETTI, B. J. 1985. Oxygen diffusion in amphiboles. *Geochimica et Cosmochimica Acta*, **49**, 1403–1411.

FORTIER, S. M. & GILETTI, B. J. 1991. Volume of self-diffusion of oxygen in biotite, muscovite and phlogopite micas. *Geochimica et Cosmochimica Acta*, **55**, 1319–1330.

FREER, R., WRIGHT, K., KROLL, H. & GOTTLICHER, J. 1997. Oxygen diffusion in sanidine feldspar and a critical appraisal of oxygen isotope-mass-effect measurements in non-cubic materials. *Philosophical Magazine*, **A75**, 485–503.

GHIORSO, M. S. & SACK, R. O. 1995. Chemical mass-transfer in magmatic processes. 4. A revised and internally consistent thermodynamic model for the interpolation and extrapolation of liquid–solid equilibria in magmatic systems at elevated temperatures and pressures. *Contributions to Mineralogy and Petrology*, **119**, 197–212.

GILETTI, B. J. & YUND, R. A. 1984. Oxygen diffusion in quartz. *Journal of Geophysical Research*, **89**, 4039–4046.

GILETTI, B. J., SEMET, M. P. & YUND, R. A. 1978. Studies in diffusion – III. Oxygen in feldspars: an ion microprobe determination. *Geochimica et Cosmochimica Acta*, **42**, 45–57.

GRIPP, A. E. & GORDON, R. G. 2002. Young tracks of hotspots and current plate velocities. *Geophysical Journal International*, **150**, 321–361.

HEARN, P. P., JR, STEINKAMPF, W. C., HORTON, D. G., SOLOMON, G. C., WHITE, L. D. & EVANS, J. R. 1989. Oxygen-isotope composition of ground water and secondary minerals in Columbia Plateau basalts: implications for the paleohydrology of the Pasco Basin. *Geology*, **17**, 606–610.

HILDRETH, W. 1981. Gradients in silicic magma chambers: implications for lithospheric magmatism. *Journal of Geophysical Research*, **86**, 10,153–10,192.

HILDRETH, W., CHRISTIANSEN, R. L. & O'NEIL, J. R. 1984. Catastrophic isotopic modification of rhyolitic magma at times of caldera subsidence, Yellowstone Plateau volcanic field. *Journal of Geophysical Research*, **89**, 8339–8369.

HILDRETH, W., HALLIDAY, A. N. & CHRISTIANSEN, R. L. 1991. Isotopic and chemical evidence concerning the genesis and contamination of basaltic and rhyolitic magma beneath Yellowstone Plateau volcanic field. *Journal of Petrology*, **32**, 63–138.

HILL, D. P. & PAKISER, L. C. 1967. Seismic-refraction study of crustal structure between the Nevada Test Site and Boise, Idaho. *Geological Society of America Bulletin*, **78**, 685–704.

HONJO, N., BONNICHSEN, B., LEEMAN, W. P. & STORMER, J. C., JR. 1992. High-temperature rhyolites from the central and western Snake River Plain. *Bulletin of Volcanology*, **54**, 220–237.

HORTON, T. W., SJOSTROM, D. J., ABRUZZESE, M. J., POAGE, M. A., WALDBAUER, J. R., HREN, M., WOODEN, J. & CHAMBERLAIN, C. P. 2004. Spatial and temporal variation of Cenozoic surface elevation in the Great Basin and Sierra Nevada. *American Journal of Science*, **304**, 862–888.

HUENGES, E., ERZINGER, J., KUCK, J., ENGESER, B. & KESSELS, W. 1997. The permeable crust: geohydraulic properties down to 9101 m depth. *Journal of Geophysical Research*, **102**, 18,255–18,265.

HUGHES, S. S. & MCCURRY, M. 2002. Bulk major and trace element evidence for a time – space evolution of Snake River Plain rhyolites, Idaho. *In*: BONNICHSEN, B., MCCURRY, M. & WHITE, C. M. (eds) *Tectonic and Magmatic Evolution of the Snake River Plain volcanic province*. Idaho Geological Survey Bulletin, **30**, 161–176.

HUPPERT, H. E. & SPARKS, R. S. J. 1988. The generation of granitic magmas by intrusion of basalt into continental crust. *Journal of Petrology*, **29**, 599–624.

INGEBRITSEN, S. E. & MANNING, C. E. 1999. Geological implications of a permeability – depth curve for the continental crust. *Geology*, **27**, 1107–1110.

JACKSON, M. D., CHEADLE, M. J. & ATHERTON, M. P. 2003. Quantitative modeling of granitic melt generation and segregation in the continental crust. *Journal of Geophysical Research*, **108**, 2332, DOI: 10.1029/2001JB001050.

KAVANAGH, J. L., MENAND, T. & SPARKS, R. S. J. 2006. An experimental investigation of sill formation and propagation in layered elastic media. *Earth and Planetary Science Letters*, **245**, 799–813.

KOJITANI, H. & AKAOJI, M. 1994. Calorimetric study of olivine solid solution in the system Mg_2SiO_4–Fe_2SiO_4. *Physics and Chemistry of Minerals*, **20**, 536–540.

LACHENBRUCH, A. H., SASS, J. H., MONROE, R. J. & MOSES, T. H., JR. 1976. Geothermal setting and simple magmatic models for Long Valley caldera. *Journal of Geophysical Research*, **81**, 769–784.

LEEMAN, W. P. 1982. Development of the Snake River Plain – Yellowstone Plateau province, Idaho and Wyoming: an overview and petrologic model. *In*: BONNICHSEN, B. & BRECKENRIDGE, R. M. (eds) *Cenozoic Geology of Idaho*. Idaho Bureau of Mines and Geology Bulletin, **26**, 155–177.

LEEMAN, W. P. & VITALIANO, C. J. 1976. Petrology of Mckinney – Basalt, Snake-River – Plain, Idaho. *Geological Society of America Bulletin*, **87**, 1777–1792.

LEEMAN, W. P., MENZIES, M. A., MATTY, D. J. & EMBREE, G. F. 1985. Strontium, neodymium, and lead isotopic compositions of deep crustal xenoliths from the Snake River Plain: evidence for Archean basement. *Earth and Planetary Science Letters*, **75**, 354–368.

LEEMAN, W. P., OLDOW, J. S. & HART, W. K. 1992. Lithosphere-scale thrusting in the western U.S. Cordillera as constrained by Sr and Nd isotopic transitions in Neogene volcanic rocks. *Geology*, **20**, 63–66.

MABEY, D. R. 1982. Geophysics and tectonics of the Snake River Plain, Idaho. *In*: BONNICHSEN, B. &

BRECKENRIDGE, R. M. (eds) *Cenozoic Geology of Idaho*. Idaho Bureau of Mines and Geology Bulletin, **26**, 139–153.

MANKINEN, E., HILDEBRAND, T. G., ZIENTEK, M. L., BOX, S. E., BOOKSTROM, A. A., CARLSON, M. H. & LARSEN, J. C. 2004. *Guide to Geophysical Data for the Northern Rocky Mountains and Adjacent Areas, Idaho, Montana, Washington, Oregon, and Wyoming*. U.S. Geological Survey Open-File Reports, **2004-1413**.

MANNING, C. E. & INGEBRITSEN, S. E. 1999. Permeability of the continental crust: implications of geothermal data and metamorphic systems. *Reviews in Geophysics*, **27**, 127–150.

MANNING, D. A. C. 1981. The effect of fluorine on liquidus phase relationships in the system qz-ab-or with excess water at 1 kb. *Contributions to Mineralogy and Petrology*, **76**, 206–215.

MCCURRY, M., HAYDEN, K. P., MORSE, L. H. & MERTZMAN, S. 2008. Genesis of post-hotspot A-type rhyolite of the Eastern Snake River Plain volcanic field by extreme fractional crystallization of olivine tholeiite. *Bulletin of Volcanology*, **70**, 361–368, DOI: 10.1007/s0445-007-0143-4.

MENZIES, M. A., LEEMAN, W. P. & HAWKESWORTH, C. J. 1984. Geochemical and isotopic evidence for the origin of continental flood basalts with particular reference to the Snake River Plain, Idaho, USA. *Transactions of the Royal Society of London*, **A310**, 643–660.

MORGAN, L. A. & MCINTOSH, W. C. 2005. Timing and development of the Heise volcanic field, Snake River Plain, Idaho, western USA. *Geological Society of America Bulletin*, **117**, 288–306.

NASH, B. P., PERKINS, M. E., CHRISTENSEN, J. N., LEE, D.-C. & HALLIDAY, A. N. 2006. The Yellowstone hotspot in space and time: Nd and Hf isotopes in silicic magmas. *Earth and Planetary Science Letters*, **247**, 143–156.

PAKISER, L. C. 1989. Geophysics of the Intermontane system. *In*:PAKISER, L. C. & MOONEY, W. D. (eds) *Geophysical Framework of the Continental United States*. Geological Society of America Memoirs, **172**, 235–247.

PATIÑO DOUCE, A. E. 1997. Generation of metaluminous A-type granites by low-pressure melting of calc-alkaline granitoids. *Geology*, **25**, 743–746.

PENG, X. & HUMPHREYS, E. D. 1998. Crustal velocity structure across the eastern Snake River Plain and the Yellowstone swell. *Journal of Geophysical Research*, **103**, 7171–7186.

PERKINS, M. E. & NASH, W. P. 2002. Explosive silicic volcanism of the Yellowstone hotspot: The ash fall tuff record. *Geological Society of America Bulletin*, **114**, 367–381.

PERKINS, M. E., NASH, W. P., BROWN, F. H. & FLECK, R. J. 1995. Fallout tuffs of Trapper Creek, Idaho – a record of Miocene explosive volcanism in the Snake River Plain volcanic province. *Geological Society of America Bulletin*, **107**, 1484–1506.

PETFORD, N. & GALLAGHER, K. 2001. Partial melting of mafic (amphibolitic) lower crust by periodic influx of basaltic magma. *Earth and Planetary Science Letters*, **193**, 483–499.

PIERCE, K. L. & MORGAN, L. A. 1992. The track of the Yellowstone hot spot: Volcanism, faulting, and uplift. *In*: LINK, P., KUNTZ, M. A. & PLATT, L. B. (eds) *Regional Geology of Eastern Idaho and Western Wyoming*. Geological Society of America Memoirs, **179**, 1–53.

RIGHTMIRE, C. T., YOUNG, H. W. & WHITEHEAD, R. L. 1976. *Geothermal Investigations in Idaho*. US Geological Survey and Idaho Department of Water Resources, Boise, ID, Water Information Bulletins, **30**, 1–28.

RODGERS, D. W., ORE, H. T., BOBO, R. T., MCQUARRIE, N. & ZENTNER, N. 2002. Extension and subsidence of the eastern Snake River Plain, Idaho. *In*: BONNICHSEN, B., MCCURRY, M. & WHITE, C. M. (eds) *Tectonic and Magmatic Evolution of the Snake River Plain Volcanic Province.* Idaho Geological Survey Bulletins, **30**, 121–155.

RYAN, M. P. 1987. Elasticity and contractancy of hawaiian olivine tholeiite and its role in the stability and structural evolution of subcaldera magma reservoirs and rift systems. *In*: DECKER, R. W., WIGHT, T. L. & STAUFFER, P. H. (eds) *Volcanism in Hawaii*. US Geological Survey Professional Papers, **1350**, 1395–1447.

SHERVAIS, J. W., VETTER, S. K. & HANAN, B. B. 2006. Layered mafic sill complex beneath the eastern Snake River Plain: evidence from cyclic geochemical variations in basalt. *Geology*, **34**, 365–368.

SMITH, R. B. & BRAILE, L. W. 1994. The Yellowstone hotspot. *Journal of Volcanology and Geothermal Research*, **61**, 121–187.

SPARLIN, M. A., BRAILE, L. W. & SMITH, R. B. 1982. Crustal structure of the eastern Snake River Plain determined from ray trace modeling of seismic refraction data. *Journal of Geophysical Research*, **87**, 2619–2633.

TAYLOR, S. R. & MCLENNAN, S. M. 1985. *The Continental Crust: its Composition and Evolution*. Blackwell, Oxford.

THOMPSON, R. N. 1975. Primary basalts and magma genesis II. Snake River Plain, Idaho, U.S.A. *Contributions to Mineralogy and Petrology*, **52**, 213–232.

VAZQUEZ, J. A. & REID, M. R. 2002. Time scales of magma storage and differentiation of voluminous high-silica rhyolites at Yellowstone caldera, Wyoming. *Contributions to Mineralogy and Petrology*, **144**, 274–285.

WAITE, G. P., SMITH, R. B. & ALLEN, R. M. 2006. V_P and V_S structure of the Yellowstone hot spot from teleseismic tomography: evidence for an upper mantle plume. *Journal of Geophysical Research*, **111**, B04303, DOI: 10.1029/2005JB003867.

WOOD, S. H. & CLEMENS, D. M. 2002. Geologic and tectonic history of the western Snake River Plain, Idaho and Oregon. *In*: BONNICHSEN, B., MCCURRY, M. & WHITE, C. M. (eds) *Tectonic and Magmatic Evolution of the Snake River Plain Volcanic Province*. Idaho Geological Survey Bulletins, **30**, 69–103.

WOODEN, J. L. & MUELLER, P. A. 1988. Pb, Sr, and Nd isotopic compositions of late Archean igneous rocks, eastern Beartooth Mountains: implications for crust-mantle evolution. *Earth and Planetary Science Letters*, **87**, 59–72.

WRIGHT, K. E., MCCURRY, M. & HUGHES, S. S. 2002. Petrology and geochemistry of the Miocene tuff of McMullen Creek, central Snake River Plain. *In*: BONNICHSEN, B., MCCURRY, M. & WHITE, C. M. (eds) *Tectonic and Magmatic Evolution of the Snake River Plain Volcanic Province.* Idaho Geological Survey Bulletins, **30**, 177–194.

YOUNKER, L. W. & VOGEL, T. A. 1976. Plutonism and plate tectonics: the origin of circum-Pacific batholiths. *Canadian Mineralogist*, **14**, 238–244.

YUAN, H. & DUEKER, K. 2005. P-wave tomogram of the Yellowstone plume. *Geophysical Research Letters*, **32**, L07304, DOI: 10.1029/2004GL022056.

YUND, R. A., SMITH, B. M. & TULLIS, J. 1981. Dislocation-assisted diffusion of oxygen in albite. *Physics and Chemistry of Minerals*, **7**, 185–189.

ZHENG, Y. 1993*a*. Calculation of oxygen isotope fractionation in anhydrous silicate minerals. *Geochimica et Cosmochimica Acta*, **57**, 1079–1091.

ZHENG, Y. 1993*b*. Calculation of oxygen isotope fractionation in hydroxyl-bearing silicates. *Earth and Planetary Science Letters*, **120**, 247–263.